# HIF1α-glycolysis engages activation-induced cell death to drive IFN-γ induction in hypoxic T cells

**Lewis Shi** ( ✉ Lewisshi@uabmc.edu )

  Heersink School of Medicine, University of Alabama at Birmingham (UAB-SOM)    https://orcid.org/0000-0002-5351-8730

**Hongxing Shen**

  University of Alabama at Birmingham    https://orcid.org/0000-0001-7400-6809

**Logan Mullen**

  University of Alaska

**Oluwagbemiga Ojo**

  Heersink School of Medicine, University of Alabama at Birmingham (UAB-SOM)

**Chuan Xing**

  University of Alabama at Birmingham

**Abdelrahman Yassin**

  Heersink School of Medicine, University of Alabama at Birmingham (UAB-SOM)

**Zach Lewis**

  Heersink School of Medicine, University of Alabama at Birmingham (UAB-SOM)

**James Bonner**

  Heersink School of Medicine, University of Alabama at Birmingham (UAB-SOM)

**Additional Declarations:** There is **NO** Competing Interest.

1 **HIF1α-glycolysis engages activation-induced cell death to drive IFN-γ induction in**
2 **hypoxic T cells**
3
4 Hongxing Shen[1], Logan Mullen[2], Oluwagbemiga A. Ojo[1], Chuan Xing[1], Abdelrahman Yassin[1],
5 Zach Lewis[1], James A. Bonner[1,3], and Lewis Zhichang Shi[1,3,4,5,6,*]
6 Affiliations:
7 [1]Department of Radiation Oncology, Heersink School of Medicine, University of Alabama at
8 Birmingham (UAB-SOM), Birmingham, AL 35233, USA.
9 [2]Genomics Core Laboratory, Institute of Arctic Biology, University of Alaska Fairbanks,
10 Fairbanks, Alaska, 99775, USA.
11 [3]O'Neal Comprehensive Cancer Center, UAB-SOM, USA
12 [4]Department of Microbiology and Immunology Institute, UAB-SOM, USA
13 [5]Department of Pharmacology and Toxicology, UAB-SOM, USA
14 [6]Immunology Institute, UAB-SOM, USA
15
16 *Correspondence should be addressed to:
17 Lewis Zhichang Shi, MD, PhD
18 Department of Radiation Oncology
19 The University of Alabama at Birmingham
20 1700 6th Avenue South, HSROC-2220A, Birmingham, AL 35233.
21 Phone: 205-975-0521
22 Fax: 205-975-4372
23 Email: Lewisshi@uabmc.edu.

**Abstract**

The role of HIF1$\alpha$-glycolysis in regulating IFN-$\gamma$ induction in hypoxic T cells is unknown. Given that hypoxia is a common feature in a wide array of pathophysiological contexts such as tumor and that IFN-$\gamma$ is instrumental for protective immunity, it is of great significance to gain a clear idea on this. Combining pharmacological and genetic gain-of-function and loss-of-function approaches, we find that HIF1$\alpha$-glycolysis controls IFN-$\gamma$ induction in both human and mouse T cells activated under hypoxia. Specific deletion of HIF1$\alpha$ in T cells (HIF1$\alpha^{-/-}$) and glycolytic inhibition significantly abrogate IFN-$\gamma$ induction. Conversely, HIF1$\alpha$ stabilization in T cells by hypoxia and VHL deletion (VHL$^{-/-}$) promotes IFN-$\gamma$ production. Mechanistically, reduced IFN-$\gamma$ production in hypoxic HIF1$\alpha^{-/-}$ T cells is due to attenuated activation-induced cell death but not proliferative defect. We further show that depletion of intracellular acetyl-CoA is a key metabolic underlying mechanism. Hypoxic HIF1$\alpha^{-/-}$ T cells are less able to kill tumor cells, and HIF1$\alpha^{-/-}$ tumor-bearing mice are not responsive to immune checkpoint blockade (ICB) therapy, indicating loss of HIF1$\alpha$ in T cells is a major mechanism of therapeutic resistance to ICBs. Importantly, acetate supplementation restores IFN-$\gamma$ production in hypoxic HIF1$\alpha^{-/-}$ T cells and re-sensitizes HIF1$\alpha^{-/-}$ tumor-bearing mice to ICBs, providing an effective strategy to overcome ICB resistance. Taken together, our results highlight T cell HIF1$\alpha$-anaerobic glycolysis as a principal mediator of IFN-$\gamma$ induction and anti-tumor immunity. Considering that acetate supplementation (i.e., glycerol triacetate (GTA)) is approved to treat infants with Canavan disease, we envision a rapid translation of our findings, justifying further testing of GTA as a repurposed medicine for ICB resistance, a pressing unmet medical need.

Keywords: T cell, HIF1$\alpha$, anaerobic glycolysis, IFN-$\gamma$, hypoxia, ICB, acetate supplementation

49 **Introduction**
50 Naïve T cells, upon receiving signals through T cell receptor (TCR) (signal 1), co-stimulatory
51 receptor (e.g., CD28, signal 2), and various cytokines (signal 3), are activated and differentiate
52 into distinct sub-lineages, including IFN-$\gamma$-producing $T_H1$[1], IL-17-producing $T_H17$[2], the
53 immunosuppressive FoxP3$^+$ regulatory T cells ($T_{reg}$)[3], as well as other recently-defined subsets[4].
54 Notwithstanding the essential role of these immune signals in deciding T cell fates, in recent
55 years, accumulating evidence indicates that at the fundamental level, it is the cellular
56 metabolism that orchestrates T cell activation and differentiation[5-15], by meeting their drastically
57 increased bioenergetic and biosynthetic demands[16]. Interestingly, seminal efforts from many
58 groups reveal a selective but not universal role of metabolic processes and transcriptional
59 factors in this process[4-7,10-15]. For example, we found that the initial metabolic reprogramming in
60 activated T cells, switching from fatty acid/pyruvate oxidation via the TCA cycle to the glycolytic,
61 pentose-phosphate, and glutaminolytic pathways, is primarily controlled by Myc but not HIF1$\alpha$ in
62 T cells[9], even though both are master regulators of cellular metabolism, downstream of
63 mTOR[17]. On the other hand, HIF1$\alpha$-glycolysis orchestrated a metabolic checkpoint in $T_H17$
64 differentiation and induction of $T_{reg}$ (i$T_{reg}$)[8]. However, given the shared importance of glycolysis in
65 both $T_H1$ and $T_H17$ differentiation, HIF1$\alpha$ is not required for IFN-$\gamma$ induction/$T_H1$ differentiation[8].
66 While this could be due in part to greater HIF1$\alpha$ induction in $T_H17$ cells than $T_H1$ cells[8], it is
67 noteworthy to mention that we performed those studies primarily under the regular normoxic
68 culture condition commonly established in the laboratory (21% $O_2$). It remains to be determined
69 whether and how HIF1$\alpha$ controls IFN-$\gamma$ induction in T cells, under hypoxia.
70
71 Hypoxia is a prominent feature in various physiological and pathological settings.
72 Physiologically, only the tissues directly exposed to inhaled atmospheric air (such as the upper
73 airways) have an $O_2$ level at ~21%. Most other healthy tissues experience $O_2$ deprivation
74 (hypoxia), to a certain degree. For example, the $O_2$ level in arterial blood is about ~14%[18], and
75 this is reduced to 5-6% in the interstitial space[19]. In lymphoid tissues like spleen, it is mostly ~3-
76 4%[20] but lower in the germinal center[21]. In the gastrointestinal (GI) tract that contains ~70-80%
77 of the total lymphocytes in our body[22], a wide range of $O_2$ tensions exists, being almost anoxic in
78 the lumen, where many obligate anaerobic commensal bacteria reside, and slightly increased at
79 the base of the villi[23]. The intestinal tissue, including the lamina propria where many T cells are
80 found, has an $O_2$ level of ~7%[24]. Pathologically, extreme hypoxia arises in the tumor
81 microenvironment (TME) of solid tumors (~1% $O_2$), as a result of abnormal vasculature,
82 heightened metabolic activities of tumor cells, and other factors[25]. Likewise, severe hypoxia can
83 be found in the inflammatory sites, due to edema, vasculitis, vasoconstriction (limiting oxygen
84 delivery), and recruitment of polymorphonuclear cells that consume high amounts of $O_2$[26]. As its
85 name tells, hypoxia-inducible factor (HIF)-1 $\alpha$ subunit (HIF1$\alpha$) is widely regarded as the primary
86 regulator of cellular adaptive responses to hypoxia[27]. When $O_2$ tensions are low, hydroxylation
87 of the prolyl residues of HIF1$\alpha$ by prolyl hydroxylase domain (PHD) enzymes is inhibited;
88 subsequently, recognition and ubiquitination of HIF1$\alpha$ by the von Hippel-Lindau protein
89 (VHL)[28,29] is suppressed. Additionally, hypoxia promotes the interaction between the C-terminal
90 transcriptional activation domain (C-TAD) of HIF1$\alpha$ and other transcriptional coactivators
91 through inhibiting hydroxylation of an asparagine residue within the C-TAD of HIF1$\alpha$[30]. These
92 modifications converge on the inhibition of proteasome degradation of HIF1$\alpha$, leading to
93 stabilized HIF1$\alpha$, which then translocate to the nucleus and mediate transcriptional and
94 epigenetic programs. Given the quite ubiquitous distribution of hypoxia in our body and the
95 essential role of IFN-$\gamma$ in immunity against intracellular pathogens and tumors[31], a clear
96 understanding of the role of HIF1$\alpha$-glycolysis axis in IFN-$\gamma$ induction in hypoxic T cells is of
97 utmost importance.
98

99   Here, we report that HIF1$\alpha$-anaerobic glycolysis is essential for IFN-$\gamma$ induction in T cells, under
100  hypoxia. HIF1$\alpha$ deletion (HIF1$\alpha^{-/-}$) in mouse T cells, knockdown (HIF1$\alpha^{KD}$) in human T cells, as
101  well as glycolytic inhibition with 2-DG markedly reduced IFN-$\gamma$ production in hypoxic T cells. On
102  the contrary, HIF1$\alpha$ stabilization in T cells exposed to hypoxia, deleted of VHL, or treated with
103  PHDs inhibitor (DMOG), increased their production of IFN-$\gamma$. We identified impaired activation-
104  induced cell death (AICD) but not proliferative defects in HIF1$\alpha^{-/-}$ T cells as the major cellular
105  mechanism underlying reduced IFN-$\gamma$ production. Molecularly and metabolically, this can be
106  attributed to the depleted intracellular pool of acetyl-CoA ([acetyl-CoA]), as acetate
107  supplementation replenished [acetyl-CoA], re-engaged AICD, and restored IFN-$\gamma$ induction in
108  hypoxic HIF1$\alpha^{-/-}$ T cells. As a result of reduced production of IFN-$\gamma$ and other late effector
109  cytokines (e.g., granzyme B and perforin), hypoxic HIF1$\alpha^{-/-}$ T cells were less able to kill tumor
110  cells *in vitro*. *In vivo*, tumor-bearing HIF1$\alpha^{-/-}$ mice were resistant to combined anti-CTLA-4 and
111  anti-PD-1 therapy (ICBs). Importantly, administration of acetate to tumor-bearing HIF1$\alpha^{-/-}$ mice
112  overcame this ICB resistance and restored IFN-$\gamma$ production in tumor-infiltrating T cells (TILs).
113  Collectively, our results establish T cell-intrinsic HIF1$\alpha$-glycolysis pathway as a major regulator
114  of IFN-$\gamma$ induction in hypoxic T cells. They manifest acetate supplementation as an effective
115  therapeutic strategy to bypass ICB resistance associated with HIF1$\alpha$ loss in T cells. Considering
116  acetate supplementation (GTA) is approved to treat infants with Canavan disease, our study
117  lays a solid foundation for future clinical testing of GTA as a repurposed medicine for ICB
118  resistance, a pressing unmet medical need in ICBs.
119
120  **Results**
121  ***HIF1$\alpha$ controls IFN-$\gamma$ induction in hypoxic T cells.***
122  Two early studies using human[32] and mouse non-T$_{reg}$ (CD4$^+$CD25$^-$) T cells[33] show that hypoxia
123  and HIF1$\alpha$ inhibit IFN-$\gamma$ production. But because CD4$^+$CD25$^-$ T cells contain ~40-50% already-
124  activated effector/central memory T cells (CD44$^+$)[34,35] that are equipped to produce IFN-$\gamma$, it
125  remains unknown if and how HIF1$\alpha$ and hypoxia regulate IFN-$\gamma$ induction in naïve T cells, upon
126  activation. To address this, using the genetic mice that we previously generated with HIF1$\alpha$
127  specifically deleted in T cells (hereafter, HIF1$\alpha^{-/-}$)[8], we isolated naïve CD4$^+$ T cells from wild-
128  type littermate controls (WT) and HIF1$\alpha^{-/-}$ mice and activated them with plate-bound anti-
129  CD3/CD28 and IL-2, in the presence and absence of IL-12. To directly compare the involvement
130  of HIF1$\alpha$ in IFN-$\gamma$ induction in normoxic and hypoxic T cells, these cells were cultured in a
131  regular cell culture incubator (21% O$_2$) and in a hypoxic chamber with 1% O$_2$ mimicking hypoxic
132  TME of solid tumors[25] and inflammatory sites[26]. Although IL-12 is commonly used to drive
133  optimal production of IFN-$\gamma$ (T$_H$1 differentiation) in activated T cells, we found that IFN-$\gamma$ can be
134  robustly induced without IL-12, albeit modestly reduced, as compared to IL-12-supplemented
135  condition (Fig. S1A). Given this and to limit the confounding effects from IL-12 stimulation on
136  IFN-$\gamma$ induction, we primarily focused on the condition without IL-12, reasoning that this would
137  allow us to more explicitly assess how T cell HIF1$\alpha$ regulates IFN-$\gamma$ induction. Surprisingly,
138  opposite to previous reports showing a negative role of HIF1$\alpha$ in IFN-$\gamma$ production by
139  CD4$^+$CD25$^-$ T cells[33], HIF1$\alpha$ was essential for IFN-$\gamma$ induction in naïve T cells, when activated
140  under hypoxia (Fig. 1A). This was accompanied with substantial downregulation of T-bet (Fig.
141  S1B), the master transcriptional regulator of IFN-$\gamma$ expression. Consistent with our previous
142  study[8], IFN-$\gamma$ induction in naïve T cells was unaffected by HIF1$\alpha$ deletion, under normoxia (Fig.
143  1B). To test if HIF1$\alpha$ also mediates IFN-$\gamma$ induction in human naïve CD4$^+$ T cells, upon
144  activation under hypoxia, we knocked down human HIF1$\alpha$ using retroviruses expressing
145  shRNAs against human HIF1$\alpha$, which also led to significantly reduced IFN-$\gamma$ induction (Fig. 1C).
146  To extend this to CD8$^+$ T cells, we sorted naïve CD8$^+$ T cells from WT and HIF1$\alpha^{-/-}$ mice,

147 similarly activated them under hypoxia, and analyzed their IFN-$\gamma$ production. As shown in Fig.
148 S1C, IFN-$\gamma$ induction was reduced in HIF1$\alpha^{-/-}$ CD8$^{\square}$ T cells as well. These results together
149 establish a selective role of HIF1$\alpha$ in IFN-$\gamma$ induction in hypoxic but not normoxic T cells[8].
150
151 To shed mechanistic light on this, we conducted whole transcriptome analysis (RNA-Seq) using
152 total RNAs isolated from WT and HIF1$\alpha^{-/-}$ T cells that were activated, under normoxia and
153 hypoxia for 48h. We chose this timepoint because it immediately precedes IFN-$\gamma$ induction that
154 occurs during the late-stage of T cell activation from Day 3-6, allowing us to establish a temporal
155 relationship of HIF1$\alpha$-mediated transcriptional and metabolic changes to subsequent IFN-$\gamma$
156 induction. Also, activated T cells rapidly die around 56h after activation through AICD (see
157 below), and 48h will maximize cell yield for downstream biochemical analyses. Whereas
158 normoxic HIF1$\alpha^{-/-}$ T cells only displayed limited transcriptomic changes (600 hits) with 37 well-
159 defined genes upregulated and 55 genes downregulated (DEGs: differentially expressed genes)
160 (Fig. S1D), in sharp contrast, there were 5168 hits in hypoxic HIF1$\alpha^{-/-}$ T cells among which 583
161 were well-defined upregulated DEGs, and 399 were downregulated DEGs (Fig. 1D). This
162 indicated a much more prominent impact of HIF1$\alpha$ in regulating transcriptomic programs in
163 hypoxic T cells than in normoxic T cells. Notably, there was very little overlap among DEGs in
164 HIF1$\alpha^{-/-}$ normoxic (Fig. S1E) vs hypoxic T cells (Fig. 1E), with top 50 genes shown in
165 heatmaps, highlighting a rather distinct role of HIF1$\alpha$ in hypoxic T cells as compared to
166 normoxic T cells. In further support, signaling pathway enrichment analyses using
167 downregulated DEGs revealed minimal overlap as well (extended datasets, supplemental Table
168 1-2). Among the top 10 enriched downregulated pathways, HIF1$\alpha$ signaling pathway was the
169 only shared hit between hypoxic T cells (Fig. 1F) and normoxic T cells (Fig. S1F). Similarly,
170 there was barely any overlap among upregulated enriched pathways between HIF1$\alpha^{-/-}$
171 normoxic and hypoxic T cells (Fig. S1G, extended dataset, supplemental Table 1-2). A closer
172 look at the other top 9 altered pathways in HIF1$\alpha^{-/-}$ hypoxic T cells showed that all of them are
173 either directly involved in (#2, #3, #4, #7-10) or intimately interacted with cellular metabolism (#5
174 and #6), suggesting an essential role of HIF1$\alpha$ in orchestrating metabolic reprogramming in
175 hypoxic T cells. In line with our previous report of a non-essential role of HIF1$\alpha$ in metabolic
176 reprogramming in activated normoxic T cells[9], none of these metabolic pathways appeared to
177 be top hits in HIF1$\alpha^{-/-}$ normoxic T cells. Among all these highly intertwined metabolic processes
178 (pentose phosphate pathway, central carbon metabolism, fructose and mannose metabolism,
179 galactose metabolism, etc.), glycolysis was the most impacted metabolic pathway in hypoxic
180 HIF1$\alpha^{-/-}$ T cells (#2) (Fig. 1F), with many of the most significantly altered genes being in this
181 pathway (e.g., *Slc2a3*, *Slc16a3*, *Tpi1*, *Slc2a1*, *Eno1*, *Pkm*, *Hk2*, *Ldha*, *Gpi1*, *Gapdh*, *Aldoc*, etc.,
182 Fig. S1H). Although the role of glycolysis[7], under the control of LDHa[36] (the enzyme catalyzing
183 the inter-conversion step of pyruvate to lactate in glycolysis) but not HIF1$\alpha$[8], has been reported
184 in IFN-$\gamma$ induction in normoxic T cells, whether HIF1$\alpha$- glycolysis controls IFN-$\gamma$ induction in
185 hypoxic T cells is not defined.
186
187 To address this and inspired by the greatly inhibited IFN-$\gamma$ induction and impacted glycolysis in
188 hypoxic HIF1$\alpha^{-/-}$ T cells, we first directly confirmed the downregulated glycolytic pathway in
189 HIF1$\alpha^{-/-}$ T cells by assessing mRNA expression of prototypical glycolytic molecules with real-
190 time RT-PCR, all of which showed drastic downregulations in hypoxic HIF1$\alpha^{-/-}$ T cells (Fig. 1G).
191 Although there were somewhat downregulations of these genes in normoxic HIF1$\alpha^{-/-}$ T cells as
192 well, they were very modest, with quite a few being less than 2-fold (Fig. 1G), confirming a
193 minor or no effect of HIF1$\alpha$ deletion on the glycolytic pathway in normoxic T cells, as indicated
194 by our RNA-Seq analyses (Fig. S1F). Robust reductions of selected glycolytic molecules on
195 protein level (i.e., Glut1–the major glucose transporter in T cells, hexokinase 2 (HK2)–a critical

196 rate-limiting glycolytic enzyme catalyzing hexose phosphorylation, and LDHa) were also
197 observed in hypoxic HIF1$\alpha^{-/-}$ T cells (Fig. 1H). We reasoned this was due to HIF1$\alpha$ stabilization
198 by hypoxia (Fig. 1H) and thereby, HIF1$\alpha$ deletion left a more prominent impact on glycolysis in
199 hypoxic T cells. To link HIF1$\alpha$-glycolysis pathway to IFN-$\gamma$ induction, we posit that hypoxic T
200 cells with more potent HIF1$\alpha$ signaling and enhanced glycolysis[37] would produce greater
201 amount of IFN-$\gamma$ than normoxic T cells, which was shown to be the case (Fig. 1I). As a
202 complementary genetic gain-of-function (GOF) approach, we generated mice with conditional
203 deletion of VHL in T cells, a primary negative regulator of HIF1$\alpha$[28,29] (hereafter, VHL$^{-/-}$). Isolated
204 naïve T cells from WT and VHL$^{-/-}$ mice were similarly activated. As expected, VHL$^{-/-}$ T cells
205 harbored stabilized HIF1$\alpha$ and upregulated Glut1, a downstream targe of HIF1$\alpha$. Like the
206 functional GOF of HIF1$\alpha$ by hypoxia, genetic GOF of HIF1$\alpha$ by VHL deletion in T cells promoted
207 IFN-$\gamma$ production, as early as day 2 when minimal IFN-$\gamma$ production can be detected in WT T
208 cells, following activation (Fig. 1J). To pinpoint a role of glycolysis in this process, we treated T
209 cells activated under hypoxia with 2-DG, a well-established glycolytic inhibitor. Clearly, 2-DG
210 almost completely abolished IFN-$\gamma$ induction in both mouse (Fig. 1K) and human T cells (Fig.
211 1L), pointing to an essential role of glycolysis in governing IFN-$\gamma$ induction in hypoxic T cells. In
212 contrast, DMOG, a cell permeable, competitive inhibitor of PHDs that stabilizes HIF1$\alpha$,
213 promoted IFN-$\gamma$ induction (Fig. 1H). Lastly, to rule out the possibility of reduced IFN-$\gamma$ in HIF1$\alpha^{-/-}$
214 T cells is due to differentially secreted factors, we mixed WT naïve CD45.1 T cells equally with
215 either CD45.2 WT/ HIF1$\alpha^{-/-}$ naïve T cells, similarly activated under hypoxia, followed by
216 detection of IFN-$\gamma$. As shown in Fig. 1M, introduction of WT CD45.1 T cells (and thus secreted
217 factors by WT T cells) did not alter reduced IFN-$\gamma$ induction in HIF1$\alpha^{-/-}$ T cells, suggesting this is
218 a T cell-autonomous phenotype.
219
220 To gain a more complete picture of how HIF1$\alpha$ in T cell affects the effector function of hypoxic T
221 cells upon activation, we analyzed other cytokines. Similar to reduced IFN-$\gamma$ production, HIF1$\alpha^{-/-}$
222 hypoxic T cells produced significantly less amount of perforin (Prf) and granzyme (GzmB)
223 (Fig. S1J), another two widely-regarded effector cytokines. Intriguingly, IL-2, a cytokine linked to
224 early-stage of T cell activation[38], was actually increased in HIF1$\alpha^{-/-}$ T cells (Fig. S1K), so was 2-
225 DG-pretreated T cells (Fig. S1L), accentuating that HIF1$\alpha$-glycolysis negatively regulates IL-2
226 production in activated T cells. Since IFN-$\gamma$, Prf, and GzmB are typically associated with late-
227 stage of T cell activation (note: they were barely detectable on Day 2-3, while abundant IL-2 can
228 be detected at this time) (data not shown), these results unveil a reciprocal regulation of late vs
229 early cytokines by HIF1$\alpha$-glycolysis in hypoxic T cells, upon activation. In support of this
230 conception, HIF1$\alpha$ stabilization by hypoxia (Fig. S1M) or VHL deletion in T cell (Fig. S1N)
231 increased Prf and GzmB but decreased IL-2 production. Taken together, our study establishes
232 HIF1$\alpha$-aerobic glycolysis as a bona fide mediator of IFN-$\gamma$ induction in hypoxic T cells.
233
234 ***Direct regulation of IFN-$\gamma$ induction by HIF1$\alpha$ and acetyl-CoA in hypoxic T cells***
235 Our above results support a crucial role of T cell HIF1$\alpha$-glycolysis in controlling IFN-$\gamma$ induction
236 in hypoxic T cells. We attempted to pinpoint a specific glycolytic mechanism, downstream of
237 HIF1$\alpha$, that drives IFN-$\gamma$ induction in T cells, under hypoxia. To this end, we overexpressed
238 individual key glycolytic molecules, i.e., Glut1, PKM2, LDHA, and MCT4, with a special focus on
239 LDHa, considering an early study showing LDHa dictates IFN-$\gamma$ induction in normoxic T cells[36],
240 However, successful overexpression of any of these individual molecules, including LDHa, in
241 HIF1$\alpha^{-/-}$ hypoxic T cells (Fig. S2A) did not rescue impaired IFN-$\gamma$ induction (Fig. S2B), arguing
242 that this is unlikely mediated by individual glycolytic checkpoints but rather the whole-spectrum
243 suppression of anaerobic glycolysis from the loss of HIF1$\alpha$ in T cells. To directly establish the
244 role of HIF1$\alpha$ in inducing IFN-$\gamma$ expression, we re-expressed HIF1$\alpha$ in HIF1$\alpha^{-/-}$ T cells, using

245  two complementary approaches: overexpression of either WT HIF1$\alpha$ or hydroxylation-defective
246  triple mutant HIF1$\alpha$ (P402A/P577A/N813A) that is stabilized and thereby remains constitutively
247  active (HIF1$\alpha$-TM)[39]. We achieved successful re-expression of HIF1$\alpha$ in hypoxic T cells with
248  either WT HIF1$\alpha$ or HIF1$\alpha$-TM (Fig. 2A). Importantly, this effectively re-stored IFN-$\gamma$ production
249  in HIF1$\alpha^{-/-}$ T cells to a level comparable to that in WT T cells (Fig. 2B). Together with the
250  drastically reduced IFN-$\gamma$ production in HIF1$\alpha^{-/-}$ T cells, these results highlight that HIF1$\alpha$ is not
251  only necessary but also sufficient to drive IFN-$\gamma$ induction in hypoxic T cells.
252
253  A direct consequence of the significantly decreased glycolytic activity is the depletion of
254  intracellular pool of acetyl-CoA ([acetyl-CoA])[36,40]. Intrigued by a recent study showing that
255  [acetyl-CoA] is instrumental for IFN-$\gamma$ induction in normoxic LDHa$^{-/-}$ T cells[36], we asked if this is
256  also responsible for impaired IFN-$\gamma$ induction in hypoxic HIF1$\alpha^{-/-}$ T cells. To test this, we
257  measured [acetyl-CoA] and found it was markedly reduced in hypoxic HIF1$\alpha^{-/-}$ T cells (Fig. 2C).
258  Acetyl-CoA can be regenerated from acetate by acetyl-CoA synthetase independent of citrate
259  release from mitochondria. We added acetate to the cultures of activated WT and HIF1$\alpha^{-/-}$ T
260  cells on Day 2, prior to appreciable IFN-$\gamma$ induction on Day 3. Cells were harvested on Day 5 to
261  measure [acetyl-CoA] and detect IFN-$\gamma$ production. As shown in Fig. 2D, acetate
262  supplementation increased [acetyl-CoA] in HIF1$\alpha^{-/-}$ T cells to that of WT T cells.  More
263  importantly, this fully restored IFN-$\gamma$ production in HIF1$\alpha^{-/-}$ T cells (Fig. 2E), supporting that the
264  maintenance of [acetyl-CoA] in hypoxic T cells by HIF1$\alpha$-anaerobic glycolysis is a major
265  metabolic mechanism underpinning IFN-$\gamma$ induction. Since IFN-$\gamma$ has long been known to be
266  essential for anti-tumor responses[41-43], we evaluated the ability of HIF1$\alpha^{-/-}$ T cells to kill tumor
267  cells by co-culturing activated WT or HIF1$\alpha^{-/-}$ hypoxic T cell with MB49 bladder tumor cells at a
268  ratio of 2:1. Cell death of MB49 cells was analyzed 48h later by staining for Annexin V and 7-
269  AAD, two commonly used markers for detection of early vs late apoptotic cells. As shown in Fig.
270  2F, HIF1$\alpha^{-/-}$ T cells were less able to kill tumor cells, as compared to WT T cells (Fig. 2F).
271  When T cells harvested from these co-cultures were analyzed for their IFN-$\gamma$ production, HIF1$\alpha^{-}$
272  $^{/-}$ T cells produced much less IFN-$\gamma$ (Fig. S2C). Because acetate supplementation re-installed
273  IFN-$\gamma$ production in HIF1$\alpha^{-/-}$ T cells (Fig. 2E), we asked if this could restore their tumor-killing
274  capacity. Indeed, acetate-pretreated HIF1$\alpha^{-/-}$ T cells had greatly improved ability to kill co-
275  cultured MB49 tumor cells, approaching that of WT T cells (Fig. 2G). Collectively, these data
276  show that HIF1$\alpha$, by controlling the anaerobic glycolysis and sustaining [acetyl-CoA],
277  orchestrates effector function and tumor-killing ability of hypoxic T cells.
278
279  ***Impaired IFN-$\gamma$ induction in HIF1$\alpha^{-/-}$ T cells is not due to their proliferative defect.***
280  Next, we want to explore cellular mechanisms underlying the blocked IFN-$\gamma$ induction in hypoxic
281  HIF1$\alpha^{-/-}$ T cells. Since we previously showed that glycolysis is an essential component of
282  metabolic reprogramming during T cell activation[9], and hypoxic HIF1$\alpha^{-/-}$ T cells had drastically
283  reduced glycolysis, we posit that their activation would be substantially impaired. To test this, we
284  employed two widely used markers to assess T cell activation: inducible T-cell COStimulator
285  (ICOS) and CD25. Consistent with a largely dispensable role of HIF1$\alpha$ in the metabolic
286  reprogramming in activated T cell under normoxia[9], we did not see overtly altered expression of
287  ICOS and CD25 in normoxic HIF1$\alpha^{-/-}$, as compared to WT T cells; in stark contrast, their
288  expression was greatly reduced in hypoxic HIF1$\alpha^{-/-}$ T cells vs WT T cells (Fig. 3A). Another
289  cardinal feature of less active T cells is that they are smaller in size[44], which can be measured
290  by forward scatter (FSC). As shown in Fig. 3B, in keeping with selectively reduced activation of
291  hypoxic HIF1$\alpha^{-/-}$ T cells, only hypoxic but not normoxic HIF1$\alpha^{-/-}$ T cells were smaller than their
292  WT counterparts. To link T cell activation to the glycolytic activity in hypoxic T cells, we analyzed
293  ICOS and CD25 expression in glycolysis$^{high}$ (Glut1$^{high}$) vs glycolysis$^{low}$ (Glut1$^{low}$) T cells, which

294  showed significant reductions in both CD4$^\square$Glut1$^{low}$(Fig. S3A) as well as CD8$^\square$ Glut1$^{low}$ T cells
295  (Fig. S3B), in comparison to their Glut1$^{high}$ counterparts. Since CD25 is also regarded as a T$_{reg}$
296  marker, we ruled out the possibility that reduced CD25 expression in activated hypoxic HIF1$\alpha^{-/-}$
297  CD4$^\square$ T cells was due to the different abundance of iT$_{reg}$ by staining for FoxP3, which appeared
298  comparable (Fig. S3C). These data together showed that HIF1$\alpha$ deletion in hypoxic T cells, by
299  decreasing their glycolytic activity, leads to selectively impaired T cell activation.
300
301  As known, T cell activation initiates a series of intracellular events, engaging a multitude of
302  signaling cascades and biochemical processes that drive T cell proliferation. As such, in line
303  with the impaired activation of hypoxic HIF1$\alpha^{-/-}$ T cells, we observed much slower proliferation,
304  indicated by significantly reduced Ki-67 Fig. (S3D), a widely used marker for proliferative cells.
305  To more explicitly examine this, we stained WT and HIF1$\alpha^{-/-}$ naïve CD4$^\square$ T cells with CellTrace
306  Violet (CTV), whose dilution can distinctively label each division of cell proliferation. CTV-
307  labeled cells were activated under normoxia and hypoxia. Consistent with unaltered activation of
308  normoxic HIF1$\alpha^{-/-}$ T cells, their proliferation appeared normal, whereas a significant delayed
309  proliferation of hypoxic HIF1$\alpha^{-/-}$ CD4$^\square$ T cells was observed. This defect was evident as early as
310  day 2 (Fig. 3C), shortly after the initial T cell growth phase (~24h)[9]. Given the reported intimate
311  relationship of cell proliferation and IFN-$\gamma$ production[45], we asked if the proliferative defect in
312  hypoxic HIF1$\alpha^{-/-}$ T cells could be responsible for reduced IFN-$\gamma$ production, by directly
313  comparing IFN-$\gamma$ production in WT and HIF1$\alpha^{-/-}$ T cells within the same division. As shown in
314  Fig.  3D and S3E, HIF1$\alpha^{-/-}$ T cells exhibited reduced IFN-$\gamma$ production, regardless of their
315  division, indicating proliferative defect in HIF1$\alpha^{-/-}$ CD4$^\square$ T cells is not a main cellular mechanism.
316
317  ***HIF1$\alpha$-glycolysis-driven AICD controls IFN-$\gamma$ induction in hypoxic T cells.***
318  Another major outcome following T cell activation is AICD, which is commonly regarded as a
319  housekeeping process to remove obsolete effector T cells during the contraction phase after a
320  successful immune response. When gone awry, this would disrupt the immune homeostasis,
321  causing autoimmune diseases[46] and/or breaching transplantation tolerance[47]. However, whether
322  AICD governs the formation of effector T cells (e.g., IFN-$\gamma$ producing T$_H$1 cells) is unknown.
323  Considering the weaker activation of hypoxic HIF1$\alpha^{-/-}$ T cells, we contemplated that this would
324  dampen AICD. To gain a complete idea of this dynamic process, we conducted a time-course
325  study, wherein apoptosis of activated WT and HIF1$\alpha^{-/-}$ T cells was measured by staining for
326  Annexin V and 7-AAD, the main form of cell death underpinning AICD[47]. While not much cell
327  death was observed on Day 1 and Day 2 following T cell activation, it rapidly arose on Day 3 in
328  WT T cells (approximately 56h post-activation), and very few cells remained alive (only ~9%,
329  Fig. S4A); this process was considerably delayed in HIF1$\alpha^{-/-}$ T cells, with > 40% of cells staying
330  alive on Day 3. Similar trends persisted on Day 4 and Day 5. Because HIF1$\alpha^{-/-}$ T cells were less
331  metabolically active and hence consumed less nutrients in the medium, we wondered if the
332  improved survival of HIF1$\alpha^{-/-}$ T cells was simply because they had more nutrients to support
333  their survival. To test this, we replaced half of the old media with fresh media daily and found
334  that this did not change the inhibited AICD in hypoxic HIF1$\alpha^{-/-}$ T cells (Fig. S4B), arguing
335  against a role of differential nutritional statuses of the cultures in this process. In addition, since
336  activated HIF1$\alpha^{-/-}$ T cells produce more IL-2 that has long been known as a growth factor for T
337  cells[47], we wondered if this would enable HIF1$\alpha^{-/-}$ T cells to survive better. We blocked IL-2 with
338  an effective neutralizing anti-IL2 antibody that we previously used[48], which did not rectify
339  inhibition of AICD in HIF1$\alpha^{-/-}$ T cells (Fig. S4C). Furthermore, given an established role of IFN-$\gamma$
340  in driving AICD[49], we wondered if reduced IFN-$\gamma$ in hypoxic HIF1$\alpha^{-/-}$ T cells could contribute to
341  this phenotype. We thus added recombinant IFN-$\gamma$ to WT and HIF1$\alpha^{-/-}$ T cell activated under
342  hypoxia. As shown in Fig. S4D, even high doses of exogenous IFN-$\gamma$ did not rescue the delay of

343    AICD in HIF1$\alpha^{-/-}$ T cells. Together, these results suggest that inhibited AICD in hypoxic HIF1$\alpha^{-/-}$
344    T cells is an unlikely outcome of altered extrinsic factors but rather a direct consequence of
345    intrinsic alterations (e.g., decreased glycolytic activity). In support of this, glycolytic inhibition
346    with 2-DG blocked AICD and improved survival of hypoxic T cells (Fig. 4A) upon activation.
347    Similar effect of 2-DG was also observed in hypoxic human T cell (Fig. S4E).
348
349    We hypothesized that impaired AICD in HIF1$\alpha^{-/-}$ hypoxic T cells may drive reduced IFN-$\gamma$
350    production. In support of this hypothesis, first, we observed a direct correlation of selectively
351    reduced IFN-$\gamma$ induction and impaired AICD in hypoxic HIF1$\alpha^{-/-}$ T cells (Fig. 4B), whereas in
352    normoxic T cells there was no impairment of ACID and therefore, no reduction of IFN-$\gamma$
353    production. Second, we directly assess the role of AICD in IFN-$\gamma$ induction by treating hypoxic T
354    cells with z-VAD-fmk, a cell-permeable, irreversible pan-caspase inhibitor that blocks all
355    features of apoptosis and AICD[47]. As expected, z-VAD-fmk substantially improved the survival
356    of activated WT T cells (Fig. 4C) and importantly, this markedly reduced IFN-$\gamma$ production in WT
357    hypoxic T cells (Fig. 4D), strongly supporting a positive role of AICD in driving IFN-$\gamma$ induction in
358    hypoxic T cells. Moreover, despite the already very low level of IFN-$\gamma$ produced by HIF1$\alpha^{-/-}$ T
359    cells, z-VAD-fmk further reduced this (Fig. 4D), in line with a modest yet significant suppression
360    of AICD in HIF1$\alpha^{-/-}$ T cells. Third, considering that acetate supplementation rescued impaired
361    IFN-$\gamma$ induction in hypoxic HIF1$\alpha^{-/-}$ T cells, we wondered if this was mediated by re-engaging
362    AICD. To test this, we activated HIF1$\alpha^{-/-}$ T cells under hypoxia, with or without acetate
363    supplementation, followed by detection of AICD on Day 3 and IFN-$\gamma$ production on Day 5.
364    Clearly, acetate supplementation greatly increased AICD in HIF1$\alpha^{-/-}$ T cells (Fig. 4E) and
365    concomitantly, augmented IFN-$\gamma$ production (Fig. 4F). Taken together, these results indicate that
366    HIF1$\alpha$-glycolysis-acetyl CoA drives AICD in hypoxic T cells and induces IFN-$\gamma$ production,
367    lacking which led to impaired AICD and IFN-$\gamma$ induction.
368
369    ***Loss of HIF1α selectively impaired IFN-$\gamma$ production in TILs***
370    Having demonstrated a selective role of HIF1$\alpha$ in controlling IFN-$\gamma$ induction in hypoxic T cells *in*
371    *vitro*, we wanted to recapitulate this *in vivo*.  As known, TME in solid tumors is a highly hypoxic
372    milieu, with O$_2$ levels being ~1%[25]; on the other hand, peripheral lymphoid organs, like spleens
373    and draining lymph nodes (DLNs), represent more oxygenated environments, although their O$_2$
374    tensions are also below 21%[20,21]. We reason that T cells from spleens/DLNs and TILs form a
375    natural, albeit not ideal, *in vivo* system to evaluate how HIF1$\alpha$ controls IFN-$\gamma$ production in T
376    cells under normoxia vs hypoxia. To this end, we inoculated WT and HIF1$\alpha^{-/-}$ mice with MB49
377    bladder tumor cells. Once established tumors formed, tumor-bearing mice were euthanized to
378    harvest TILs and T cells from spleens and DLNs, followed by analyses of IFN-$\gamma$ production.
379    Whereas there was no overt reduction of IFN-$\gamma$ in HIF1$\alpha^{-/-}$ CD4$^\square$ and CD8$^\square$ T cells from spleen
380    (Fig. 5A) and DLN (Fig. S5A), it was substantially decreased in HIF1$\alpha^{-/-}$  TILs (Fig. 5B), as
381    compared to their WT counterparts, corroborating our *in vitro* data showing a selective role of
382    HIF1$\alpha$ in driving IFN-$\gamma$ production in hypoxic T cells. Likewise, the production of GzmB (Fig.
383    S5B) and Prf (Fig. S5C) was significantly lower in HIF1$\alpha^{-/-}$ TILs but not T cells from spleens and
384    DLNs than their corresponding WT T cells. Also, in parallel to greater production of IFN-$\gamma$,
385    GzmB, and Prf by hypoxic T cells over normoxic T cells *in vitro*, TILs also produced those
386    cytokines at a higher level than T cells from spleens (Fig. S5D). Intrigued by these results from
387    the transplantable MB49 bladder tumor model, we wanted to further confirm this using an
388    orthotopic tumor model. To this end, we employed the well-established B16-BL6 melanoma that
389    can be established by intradermally injecting syngeneic B16-BL6 cells into B6 mice. Isolated
390    TILs and splenocytes were similarly analyzed, as aforementioned. Consistent with what we
391    observed in the MB49 bladder tumors, IFN-$\gamma$ production was also highly comparable between

392   HIF1α⁻/⁻ CD4□ and CD8□ splenocytes and their WT counterparts isolated from B16 melanoma-
393   bearing mice (Fig. 5C); a significant reduction was seen in HIF1α⁻/⁻ CD4□ and CD8□ TILs as
394   compared to WT TILs (Fig. 5D). Taken together, HIF1α is selectively required for IFN-γ
395   production in hypoxic TILs but not more oxygenated peripheral T cells.
396
397   Our *in vitro* assays showed that VHL⁻/⁻ T cells with stabilized HIF1α were predisposed to
398   produce IFN-γ as early as day 2.5, when activated under hypoxia (Fig. 1F). To determine if VHL
399   deletion in T cells would also promote IFN-γ production *in vivo*, we inoculated WT and VHL⁻/⁻
400   mice with MB49 tumor cells. Mice with established tumors were euthanized to harvest TILs and
401   T cells from spleens and DLNs. As expected and consistent with our *in vitro* data, we observed
402   increased expression of Glut1 in all VHL⁻/⁻ T cells harvested from spleen, DLNs, and tumors
403   (Fig. S5E), as a result of stabilized HIF1α in VHL⁻/⁻ T cells[8]. In parallel to our *in vitro* results,
404   there was a greater IFN-γ production in hypoxic VHL⁻/⁻ TILs than WT TILs (Fig. 5F).
405   Noteworthily, because HIF1α stabilization occurs in peripheral VHL⁻/⁻ T cells, we saw
406   significantly increased IFN-γ production even in these oxygenated T cells from spleen (Fig. 5E)
407   and DLNs (Fig. S5F). Overall, these in *vivo* results comply with our *in vitro* data, establishing a
408   pivotal role of HIF1α in controlling IFN-γ production in T cells, when it gets stabilized by hypoxia
409   (e.g., TME) or deletion of its negative regulator (e.g., VHL).
410
411   ***HIF1α in T cells governs ICB efficacy.***
412   ICBs have emerged as a major pillar of cancer care [50-55]. While functional rejuvenation (e.g. IFN-
413   γ production) of TILs by ICBs has been known to be important for their efficacy[41,43,56], specific
414   underlying mechanisms are not well-understood. Our results show that HIF1α in T cells is
415   instrumental for the effector function of TILs. We therefore asked if HIF1α in T cells would
416   represent an essential metabolic and molecular mechanism governing therapeutic effects of
417   ICBs. To test this, we treated WT and HIF1α⁻/⁻ mice bearing palpable MB49 bladder tumors
418   with combined anti-CTLA-4+anti-PD-1 (combo), a more efficacious ICB therapy than
419   monotherapies (anti-CTLA-4 or anti-PD-1 alone)[57], following the regimen that we previously
420   described[41]. As shown in Fig. 6A, while combo potently suppressed tumor growth in WT mice, it
421   failed to do so in HIF1α⁻/⁻ mice, indicating a pivotal role of T cell HIF1α in dictating ICB efficacy.
422   We euthanized these mice on day 18 and measured their tumor weights. Tumors from combo-
423   treated WT mice were visually smaller and weighed significantly less than those from combo-
424   treated HIF1α⁻/⁻ mice (Fig. 6B). When isolated T cells from these mice were analyzed for their
425   IFN-γ production, we observed a selective reduction of IFN-γ in HIF1α⁻/⁻ TILs (Fig. 6C) but not T
426   cells from spleen (Fig. S6A) or DLNs (Fig. S6B), as compared to their WT counterparts, again
427   confirming a specific role of HIF1α in hypoxic T cells. Our results are consistent with an early
428   study showing that HIF1α in CD8□ T cells is required for optimal anti-tumor immunity in
429   colorectal cancer (MC38)[58], following adoptive T-cell therapy (another major form of
430   immunotherapy) and ICBs. Together, these studies support an important role of T cell-intrinsic
431   HIF1α signaling in mediating anti-tumor immunity and ICB efficacy in various types of tumor.
432
433   A significant barrier in ICBs is the therapeutic resistance to these novel therapeutics [57,59]. Our
434   above results, together with a previous study[58], inform loss of the HIF1α signaling pathway in T
435   cells as a major mechanism of ICB resistance. However, how to overcome this ICB resistance
436   has been elusive, a solution to which would undoubtedly expand the clinical utilization of ICBs
437   and benefit more patients. Inspired by our data showing that acetate supplementation can
438   rescue reduced IFN-γ production and impaired tumor killing ability of HIF1α⁻/⁻ T cells *in vitro*, we
439   asked if this could act as an effective strategy to circumvent ICB resistance in HIF1α⁻/⁻ tumor-
440   bearing mice, *in vivo*. To this end, we administered acetate to tumor-bearing WT and HIF1α⁻/⁻

10

441  mice, followed by combo ICB treatments. While acetate supplementation alone did not improve
442  combo efficacy in WT tumor-bearing mice, remarkably, this led to greatly improved therapeutic
443  effects of combo in HIF1$\alpha^{-/-}$ mice, evidenced by greatly suppressed tumor growth (Fig. 6D),
444  reduced tumor weights (Fig. 6E), and significantly increased IFN-$\gamma$ production by HIF1$\alpha^{-/-}$ CD4$^\square$
445  (Fig. 6F) and CD8$^\square$ (Fig. S6C) TILs.
446
447  Putting everything together, we show that the HIF$\alpha$ signaling in T cells, by maintaining their
448  glycolytic activity (hence, [acetyl-CoA]) and AICD, drives IFN-$\gamma$ induction. Loss of HIF1$\alpha$ in T
449  cells impairs their tumor killing capacity and renders tumor-bearing mice resistant to ICBs, which
450  can be reversed by acetate supplementation. Considering that GTA is approved to treat infants
451  with Canavan disease (an indication of highly acceptable toxicity profile), we envision a smooth
452  translation of our findings, which can lead to a rapid repurposing of GTA as an effective
453  therapeutic intervention for ICB resistance, a pressing unmet medical need.
454
455  **Discussion**
456  Cellular metabolism emerges as the fundamental driving force in T cell activation and
457  differentiation[5-15], by supporting their drastically increased bioenergetic and biosynthetic
458  demands[16]. Despite glycolysis is a key component of this metabolic reprogramming associated
459  with T cell activation and $T_H1$ differentiation[7,36], under normoxia, this is largely independent of T
460  cell HIF1$\alpha$ but rather, actively controlled by Myc[8,9]. Given this, it remains unknown whether and
461  how T cell HIF1$\alpha$ regulates IFN-$\gamma$ induction/$T_H1$ differentiation, under hypoxia, and whether this
462  relies on anaerobic glycolysis. Considering hypoxia is a common feature in various
463  phathophysiological contexts, especially in the TME of solid tumors, the lumen of the GI tract,
464  and inflammatory sites, a clear understanding of this is importance. Using T cell-specific GOF
465  and LOF genetic systems as well as pharmacological modulators, we unveil an indispensable
466  role of T cell HIF1$\alpha$ signaling in inducing IFN-$\gamma$ production in hypoxic but not normoxic T cells,
467  upon activation, in a process dependent on AICD but not activation-driven cell proliferation.
468  Severely impaired anaerobic glycolysis in hypoxic HIF1$\alpha^{-/-}$ T cells results in depleted [acetyl-
469  CoA], and replenishment of [acetyl-CoA] with acetate supplementation restores IFN-$\gamma$ production
470  in HIF1$\alpha^{-/-}$ hypoxic T cells. Similarly, hypoxic HIF1$\alpha^{-/-}$ TILs but not oxygenated peripheral T
471  cells from spleens and DLNs have reduced IFN-$\gamma$ production. Most importantly, HIF1$\alpha^{-/-}$ mice
472  bearing established tumors are resistant to ICBs, which can be treated with acetate
473  supplementation, providing an effective strategy to overcome ICB resistance.
474
475  To the best of our knowledge, this is the first study to show that HIF1$\alpha$ is a bona fide regulator of
476  IFN-$\gamma$ induction in hypoxic T cells, supported by drastically reduced IFN-$\gamma$ production in HIF1$\alpha^{-/-}$
477  T activated under hypoxia (*in vitro*) and HIF1$\alpha^{-/-}$ TILs (*in vivo*). Conversely, HIF1$\alpha$ stabilization
478  in hypoxic T cells, TILs, and VHL$^{-/-}$ T cells significantly increased IFN-$\gamma$ induction over normoxic
479  T cells, oxygenated peripheral T cells, and T cells from littermate control mice, respectively.
480  Moreover, re-expression of HIF1$\alpha$-WT or constitutively active HIF1$\alpha$-TM in hypoxic HIF1$\alpha^{-/-}$ T
481  cells largely restores their capacity to produce IFN-$\gamma$. IFN-$\gamma$ induction in hypoxic T cells is
482  completely dependent on their glycolytic activity, as glycolytic inhibition with 2-DG abolishes it.
483  Correlatively, HIF1$\alpha$ deletion in hypoxic T cells severely downregulates glycolysis and greatly
484  depletes [acetyl-CoA]. As such, acetate supplementation, by replenishing [acetyl-CoA], restores
485  IFN-$\gamma$ production in HIF1$\alpha^{-/-}$ T cells both *in vitro* and *in vivo*. Interestingly, production of other
486  late effector cytokines (e.g., Prf and GzmB), in addition to IFN-$\gamma$, is also reduced in hypoxic
487  HIF1$\alpha^{-/-}$ T cells. In contrast, production of an early cytokine IL-2[38] is increased in HIF1$\alpha^{-/-}$ T
488  cells, pointing to a reciprocal regulatory role of HIF1$\alpha$ in late vs early cytokine production. Our
489  results seem to conflict with two previous studies[32,33] wherein a negative role of hypoxia and

11

490    HIF1α in IFN-γ production in CD4$^-$CD25$^-$ was reported. However, it is noteworthy to mention
491    that CD4$^-$CD25$^-$ cells contain ~40-50% of already activated effector/central memory T cells
492    (CD44$^-$)[34,35] that are capable of producing IFN-γ. While this discrepancy may be due to the
493    differential effect of HIF1α and hypoxia in IFN-γ production by already-activated T cells vs IFN-γ
494    induction in naïve T cells (being activated), this warrants further investigations. That said, our
495    results are in line with previous reports showing that specific deletion of VHL in T$_{reg}$ cells[60] led to
496    increased IFN-γ production, and that VHL deletion[61] or PHD deletion[62] in T cells promoted the
497    polyfunctionality of CD8$^-$ T cells (i.e., increased production of IFN-γ, TNF, and GzmB), and that
498    total (not naïve) CD8$^-$ T cells activated under hypoxia also express higher levels of IFN-γ[63].
499    Interestingly, although we show that HIF1α is dispensable for IFN-γ induction[8] and aerobic
500    glycolysis in normoxic T cells[9], a recent study reported that T cell LDHa maintains aerobic
501    glycolysis and [acetyl-CoA] in normoxic T cells, promoting IFN-γ induction and T$_H$1
502    differentiation[36]. Here, we find that HIF1α plays an essential role in IFN-γ induction in hypoxic T
503    cells, by maintaining anaerobic glycolysis and [acetyl-coA], which is largely independent of
504    LDHa, as overexpression of LDHa did not rescue the impaired IFN-γ induction in HIF1α$^{-/-}$
505    hypoxic T cells. While this can be explained to certain extent that LDHa is just one of many
506    glycolytic genes regulated by HIF1α in hypoxic T cells, these studies otherwise highlight that
507    LDHa but not HIF1α is required for IFN-γ induction in normoxic T cells, whereas HIF1α but not
508    LDHa is essential for IFN-γ induction in hypoxic T cells, although they both exert this function by
509    maintaining glycolysis and [acetyl-CoA]. To this end, we show that glycolytic inhibition with 2-DG
510    almost completely shuts down IFN-γ induction in both normoxic[8] and hypoxic T cells (this study).
511
512    We previously showed that glycolysis is an essential component of metabolic reprogramming
513    during T cell activation under normoxia, which is under primary regulation of Myc but not
514    HIF1α[9]. Acute deletion of HIF1α in normoxic T cells only led to minor or no impact on glycolysis
515    and as such, no overt changes to cell growth, cell activation, and activation-driven cell
516    proliferation were found in HIF1α$^{-/-}$ T cells[9], consistent with our results reported here. In
517    contrast, under hypoxia, HIF1α deletion in T cells impacts a multitude of metabolic processes,
518    encompassing central carbon metabolism (#3 hit), fructose and mannose metabolism (#4 hit),
519    galactose metabolism (#7 hit), and pentose phosphate pathway (#8 hit), in addition to glycolysis
520    (#2 hit), suggesting HIF1α is an important mediator of metabolic reprogramming in hypoxic T
521    cells. It would be interesting to dissect out the differential roles of HIF1α and Myc in
522    orchestrating metabolic reprogramming in T cell activated under normoxia vs hypoxia, in the
523    near future. Accompanied with reduced glycolysis pathway in hypoxic HIF1α$^{-/-}$ T cells is
524    impaired T cell activation that in turn leads to suppressed AICD and cell proliferation defect.
525    Interestingly, we find that impaired AICD but not delayed cell proliferation in HIF1α$^{-/-}$ hypoxic T
526    cells contributes to reduced IFN-γ induction, as IFN-γ reduction persists in all HIF1α$^{-/-}$ cells,
527    regardless of cell division; conversely, inhibition of AICD substantially reduces IFN-γ production
528    in WT T cells and even decreases the already low level of IFN-γ production in HIF1α$^{-/-}$ T cells.
529    We largely ruled out inhibition of AICD in HIF1α$^{-/-}$ hypoxic T cells is mediated by secreted
530    extrinsic factors, as refreshing half of the old medium daily, blocking IL-2, and adding IFN-γ to
531    HIF1α$^{-/-}$ T cell cultures could not rescue this phenotype. Our results support that this is cell-
532    autonomous outcome from decreased glycolysis and reduced [acetyl-CoA], as replenished
533    [acetyl-CoA] by acetate supplementation re-engages AICD in HIF1α$^{-/-}$ hypoxic T cells, leading
534    to their restored IFN-γ production and tumor killing capacity. Of note, AICD has long been
535    considered as a housekeeping process to eliminate unwanted effector T cells, a byproduct of a
536    successful immune response. In return, this saves space for useful T cells and maintain immune
537    homeostasis. When blocked, pathologies such as autoimmunity[46] and loss of transplantation
538    tolerance[47] arise. Our data on the other hand strongly argue for an active role of AICD in

539     promoting IFN-$\gamma$ induction in hypoxic T cells, regulated by HIF1$\alpha$-glycolysis-acetyl-CoA axis.
540     Because the Fas-FasL axis[46] is important in mediating AICD in T cells, future studies ought to
541     assess how HIF1$\alpha$ cross talks with this axis.
542
543     Unprecedented therapeutic effects of ICBs in various types of late-stage cancer have propelled
544     immunotherapy as a mainstay therapy for cancer patients[50-55]. However, their efficacy has
545     reached a plateau. For instance, even with the combination therapy of anti-CTLA-4 and anti-PD-
546     1, only ~34% of patients with advanced melanoma exhibit progression-free survival[57].
547     Functional rejuvenation of TILs by ICBs[41,43,56] has been dubbed as a major mechanism
548     underlying ICB efficacy. How to effectively boost the effector function of TILs (e.g., IFN-$\gamma$
549     production) would be key to expand the clinical successes of ICBs. Considering that TILs and
550     tumor cells co-exist in a metabolically challenging milieu characterized by hypoxia and poor
551     nutrition, substantial research endeavors in recent years have been devoted to studying the
552     intratumoral metabolic tug-of-war between TILs and tumor cells, in order to tilt it in favor of TILs.
553     To this end, an early study showed that glycolysis[high] tumors, by consuming glucose, suppress
554     the effector function of TILs, which can be reversed by ICBs (i.e., anti-CTLA-4, anti-PD-1/L1)[64].
555     However, a more recent study found that anti-CTLA-4 was only effective in glycolysis[low] tumors,
556     which the authors attributed to the preferential feeding of glucose to $T_{reg}$, leading to phenotypic
557     and functional destabilization of intratumoral $T_{reg}$ toward IFN-$\gamma$ and TNF-producing effector T
558     cells[65]. Despite the discrepancy between these two studies, it is clear that glycolysis is intimately
559     involved in shaping TILs. Our study shows that dysfunctional HIF1$\alpha$-anaerobic glycolysis in TILs
560     significantly impairs effector function of TILs, including IFN-$\gamma$ production, rendering tumor-
561     bearing mice resistant to ICBs. Together with a previous study using other tumor models, we
562     argue that T cell-intrinsic loss of HIF1$\alpha$ is a major mechanism of therapeutic resistance to ICBs.
563     Most importantly, we show that administration of acetate to HIF1$\alpha^{-/-}$ mice bearing established
564     tumors can re-sensitize them to ICBs, manifesting an effective strategy to overcome this ICB
565     resistance, a pressing unmet medical need in the clinic. Interestingly, another recent study[66]
566     reported that Warburg effect in tumor cells (reliance on glycolysis) is mainly mediated by the
567     diversion of pyruvate flux away from acetyl-CoA generation; by replenishing [acetyl-CoA],
568     acetate supplementation reverses Warburg effect and drive tumor cell differentiation, which in
569     turn suppresses tumorigenesis. This, together with the functional boosting effects of acetate
570     supplementation on TILs after ICBs, highlight acetate supplementation as an ideal "two birds, on
571     stone" strategy to boost anti-tumor responses. Given that glycerol triacetate (GTA), a form of
572     acetate supplementation, is already approved by the FDA to treat infant with Canavan disease,
573     our results justify further clinical testing of GTA as a repurposed medicine for ICB resistance.
574
575     In summary, we find that HIF$\alpha$-glycolysis, by maintaining [acetyl-CoA] and activating AICD,
576     drives IFN-$\gamma$ induction selectively in hypoxic T cells. Specific deletion of HIF1$\alpha$ in T cells largely
577     abolishes T cells' ability to kill tumor cells and tumor-bearing mice's responses to ICBs. We
578     further demonstrate that this can be recovered by acetate supplementation (Fig. S6D).

13

579 **Methods**
580 *Mice and cell lines*
581 The HIF1α$^{-\boxplus}$ mice with specific HIF1α deletion in T cells were generated by crossing floxed
582 HIF1α mice (Jackson Laboratory, Stock No.: 007561) with CD4-Cre transgenic mice (Jackson
583 Laboratory, Stock No.: 022071)[8]. VHL$^{-\boxplus}$ mice with VHL specifically deleted in T cells were
584 similarly generated by crossing floxed VHL mice (Jackson Laboratory, Stock No.: 012933) with
585 CD4-Cre transgenic mice. CD45.1 mice on B6 background (Jackson Laboratory, Stock No.:
586 002014) were procured from The Jackson Laboratory (Bar Harbor, ME) and bred in our animal
587 facility. All mice were housed in specific pathogen-free conditions in the animal facility of The
588 University of Alabama at Birmingham (UAB) under 12 hours/12 hours light/dark cycle, ambient
589 room temperature (22 °C) with 40%-70% humidity. Seven to twelve-week-old mice were used in
590 the experiments. Male mice were used for MB49 model, as MB49 tumor cell line was generated
591 in a male mouse to avoid cross-sex immune response. To facilitate random assignment of mice
592 inoculated with B16-BL6 melanoma cells to different groups, we used female mice, as adult
593 male mice typically show aggressive behaviors and could confound the experiments with
594 uneven distribution of tumor sizes. Our animal protocol (APN-21945) was approved by
595 Institutional Animal Care and Use Committee at UAB. All tumor-bearing mice were humanely
596 euthanized prior to their tumors reaching the maximally allowed tumor size (20 mm in diameter)
597 in our animal protocol. The MB49 bladder cells were kindly provided by Dr. A. Kamat at MD
598 Anderson Cancer Center. MB49 cells were cultured in DMEM supplemented with 10% FBS and
599 100 units/mL of penicillin and 100 µg/mL of streptomycin (all from Invitrogen). The B16-BL6
600 murine melanoma cells were kindly provided by Dr I. Fidler at MD Anderson Cancer Center and
601 cultured with MEM supplemented with 10% FBS, 2mM L-glutamine, 1mM sodium pyruvate, 1%
602 non-essential amino acids, 1% vitamin, 100 units/mL of penicillin and 100 µg/mL of streptomycin
603 (all from Invitrogen). All cells were cultured in a humidified 37 $\square$C incubator with 5% $CO_2$. All
604 cells were regularly tested with the MycoAlert detection kit (Lonza, LT07-118) to ensure they
605 were free of mycoplasma contamination.
606
607 *Mouse naïve T cell isolation and activation*
608 Naïve T cells were isolated from spleens and lymph nodes by negative selection using
609 microbeads following the manufacturer's instructions (Miltenyi, #130-104-453 for CD4 and #130-
610 096-543 for CD8). The purity of CD4$^+$CD62L$^{hi}$CD44$^{lo}$CD25$^-$ naïve CD4 T cells and
611 CD8$^+$CD62L$^{hi}$CD44$^{lo}$ naïve CD8 T cells were confirmed by flow cytometry. Freshly isolated
612 naïve CD4 T cells were stimulated with plate-bound anti-CD3 (Clone 145-2C11, Bio X cell,
613 #BE0001-1) and anti-CD28 (Clone 37.51, Bio X cell, #BE0015-1) in presence of 100U/mL
614 human IL-2. Plates were pre-coated with 2µg/mL anti-CD3 and anti-CD28 for at least 2h. Naïve
615 T cells were activated with plate-bond anti-CD3 plus anti-CD28 in presence of 100U/mL IL-2,
616 with 0.2ng/mL or without IL-12. For hypoxic condition, cultures were placed in a hypoxic
617 chamber with oxygen level set at 1% to mimic the $O_2$ tension in the TME of solid tumors. In
618 some experiments, 50% of old media were refreshed with freshly prepared Click's medium
619 daily. Where designated, 20mM of NaAc, 0.5 µM of 2-DG (Sigma, #8375), 0.2 µM of DMOG
620 (Sigma, #400091) or solvent control was added to the culture medium. Cell apoptosis and
621 transcription factors were checked on day 2.5 and cytokines were check on day 5.5 after a brief
622 PMA and ionomycin stimulation, as we described before[8]. For *in vitro* CD45.1/CD45.2 co-
623 culture, CD45.1 naïve CD4 T cells were equally mixed with WT or HIF1α$^{-\boxplus}$ naïve CD4$^\square$ T cells
624 (congenically labeled with CD45.2). Cells were then activated and IFN-γ was checked after PMA
625 and inonomycin stimulation. To block IL-2, cells were similarly activated, in the presence of anti-
626 mouse IL-2 (Bio X Cell, #BE0043) at 10µg/mL. To assess T cell proliferation, cells were pre-
627 labeled with 2 $\square$M CellTrace Violet (CTV, Thermo Fisher, #C34557) by incubating for 20 min
628 with periodical mixing. After incubation, cells were washed twice with complete culture medium

629  to remove soluble CTV. To set up co-culture of hypoxic T cells with MB49 cells, we activated
630  WT or HIFα⁻⁺ T cells for 5 days under hypoxia and co-cultured with MB49 tumor cells at the
631  ratio of T cell (effector): MB49 (target) of 2:1. The culture plate was pre-coated with 0.2 µg/mL of
632  anti-CD3 for 2h. Cell apoptosis of tumor cells and IFN-γ production in T cells was analyzed 48h
633  later.
634
635  ***Human naïve CD4 T cell isolation and activation, 2-DG treatment***
636  Human naïve CD4 T cells were isolated from Leukocyte Reduction System (LRS) Cones
637  (procured from Lifesouth community blood centers). Total PBMC cells were flushed from human
638  LRS cone with phosphate-buffered saline (PBS) containing 2% fetal bovine serum (FBS).
639  Centrifuge at 800 × g for 10 minutes before the lysis of red blood cells. Human naïve CD4 T
640  cells were purified by negative selection using microbeads following the manufacturer's manual
641  (Miltenyi, #130-094-131). The purity was more than 95% checked by flow cytometry. Freshly
642  isolated naïve CD4 T cells were activated with plate-bound anti-human CD3 (Clone UCHT1,
643  BioLegend, #300438) and anti-human CD28 (Clone CD28.2, BioLegend, #302934) in the
644  presence of 100 U/mL human IL-2. 0.5 µM of 2-DG or solvent control was added on day 0. To
645  knock down human *HIF1A* using shRNAs, we designed and synthesized the oligoes from IDT
646  and cloned it to retroviral vector LMP. The target sequences of human shHIF1a are sh#2
647  GGGTTGAAACTCAAGCAACTG. The inserts were validated by DNA sequencing. Retroviruses
648  were packed by co-transfection of transfer plasmid and packaging plasmid pMD2.G to phoenix
649  cells. Retroviral particles were then used to transduce activated human T cells using spin-
650  infection approach as for mouse T cells (described below).
651
652  ***Plasmid construction, virus packaging and transduction***
653  The coding sequences (CDS) of murine *Hif1α*, *Glut1*, *Pkm2*, *Ldha* and *Mct4* were PCR-
654  amplified from mouse first-strand cDNA library produced by reverse transcription (Invitrogen,
655  #11752-050) and cloned into the retroviral vector pMIG II. The inserts were validated by DNA
656  sequencing. Retrovirus was produced by co-transfection of phoenix cells with transfer plasmid
657  and packaging plasmid pCL-Eco. Virus-containing culture medium was collected at 48 and 72h
658  post-transfection. Freshly isolated naïve CD4 T cells were activated for 24h before retroviral
659  spin-infection in virus-containing culture medium with the presence of Lipofectamine 3000
660  (Invitrogen, #L3000-150) and human IL-2, as we previously described[67]. Successfully
661  transduced T cells expressing GFP were sorted by flow cytometry. The overexpression of
662  interested genes was validated by western blot. To check IFN-γ production, sorted GFP⁺ cells
663  were re-activated on 0.2 µg/mL anti-CD3 pre-coated plate for 4 days under hypoxia.
664
665  ***Cell apoptosis assay***
666  Cell apoptosis was analyzed by flow cytometry, as described before[68]. Naïve T cells were
667  activated under specified normoxic or hypoxic conditions. On day 2.5, cells were harvested,
668  washed once with DPBS and again with 1× Annexin V binding buffer before staining with
669  Annexin V (1:50, Thermo Fisher, #17-8007) and 7-AAD (1:200, Sigma, #129935) or propidium
670  iodide (1:50, Thermo Fisher, #00-6990-42) in 1× Annexin V binding buffer for 30 min at room
671  temperature. Cells were acquired by Attune NxT Flow Cytometer and data were analyzed by
672  FlowJo.
673
674  ***In vivo* tumor inoculation and treatment**
675  Mice were shaved on the right flank one day before tumor inoculation. On day 0, anesthetized
676  mice were inoculated subcutaneously with 5 × 10⁵ of MB49 cells to the right flank. Anti-CTLA-4
677  (Bio X Cell, clone 9H10) and anti-PD-1 (Bio X Cell, clone 29F.1A12) or isotype controls was
678  given by intraperitoneal injection (i.p.) on day 6, 9, and 12 at a dose of 200, 100, and 100 µg per
679  mouse, respectively, as we previously described[41]. To establish orthotopic B16-BL6 melanoma

680  model, anesthetized mice were inoculated intradermally with 1.25 × $10^5$ of B16-BL6 cells into
681  the right flanks on day 0. Tumors were measured by caliper every other day starting from day 6
682  and tumor volumes ($mm^3$) were calculated using the formula (0.52× length × $width^2$). The tumor-
683  bearing mice were sacrificed at indicated time points. Upon euthanization, tumors, tumor-
684  draining lymph nodes and spleens were collected, and tumor weights were recorded. For NaAc
685  treatment *in vivo*, mice were treated with 500 mg/kg i.p. plus drinking water containing 200mM
686  sodium acetate starting from day 3. Control mice were injected with equal volume of DPBS at
687  the same time and fed with regular drinking water.
688
689  ***TILs isolation, tumor-draining lymph nodes (dLN) and splenocyte preparation***
690  Tumors were collected into ice-cold RPMI 1640 containing 2% FBS and minced into fine pieces
691  on ice, followed by digestion with 400 U/mL collagenase D (Worthington Biochemical
692  Corporation, #LS004186) and 20 µg/mL DNase I (Sigma, #10104159001) at 37 ☐C for 40 min
693  with periodic mixing. EDTA (Sigma, #1233508) was then added to the final concentration of 10
694  mM to stop digestion. Cell suspensions were filtered through 70 µM cell strainers, and TILs
695  were obtained by collecting the cells in the interphase after Ficoll (MP Biomedicals,
696  #091692254) separation. Spleens and tumor-draining lymph nodes were collected in ice-cold
697  HBSS containing 2% FBS to prepare single cell suspensions. Cells were filtered through 70 µM
698  nylon mesh after lysis of red blood cells. TILs, dLNs and splenocytes were all re-suspended in
699  complete Click's medium (Irvine Scientific, #9195-500mL) for following staining and flow
700  cytometric analyses.
701
702  ***Flow cytometric analysis***
703  For surface staining, single cell suspensions were incubated with antibody cocktails in DPBS
704  containing 2% (wt/vol) BSA for 30 min on ice. LIVE/DEAD™ Fixable Aqua Dead Cell Stain Kit
705  (Thermo Fisher: L34957) was performed according to the manufacturer's instructions. To stain
706  transcriptional factors, cells were fixed by the fixation buffer in the FoxP3/Transcription Factor
707  Staining Buffer Set (Invitrogen, #00-5523-00) following surface staining, and stained
708  intracellularly according to the manufacturer's instructions. To detect intracellular cytokines,
709  cells were briefly stimulated for 4-5 h with phorbol 12-myristate 13-acetate (PMA, final
710  concentration: 50 ng/mL; Sigma, #P8139-5MG) plus ionomycin (final concentration: 1 ☐M;
711  Sigma, #I0634-1MG) in the presence of monensin (BD Biosciences, #51-2092KZ). Stimulated
712  cells were stained with surface markers, then fixed using the fixation buffer in the BD
713  Cytofix/Cytoperm Plus Fixation/Permeabilization Kit (BD Biosciences, #554715), and stained for
714  cytokines with corresponding antibodies ntracellularly, according to the manufacturer's
715  instructions. Used flow Antibodies are listed in the Supplemental Table. All the flow cytometric
716  data were acquired using the built-in software of the Attune NxT Flow Cytometer (Invitrogen,
717  A24860) from Thermo Fisher. Flow cytometric data were analyzed using FlowJo (version
718  10.8.1).

| Antibodies | Clone | Source | Identifier | Antibody dilution |
|---|---|---|---|---|
| Anti-Mouse CD8 Brilliant Violet 785™ | 53-6.7 | BD Biosciences | #563332 | 1/200 |
| Anti-Mouse CD4 Brilliant Violet 421™ | RM4-5 | BioLegend | #100544 | 1/200 |
| Anti-Mouse CD45 PerCP-Cyanine5.5 | 30-F11 | Thermo Fisher | #45-0451-82 | 1/200 |
| Anti-Mouse CD45.1 PerCP-Cyanine5.5 | A20 | BioLegend | #110728 | 1/200 |
| Anti-Mouse CD45.2 Alexa Fluor® 700 | 104 | BioLegend | #109822 | 1/200 |
| Anti-Mouse TCRβ APC-Cy7 | H57-597 | BioLegend | #109220 | 1/200 |
| Anti-Mouse Perforin PE | S16009A | BioLegend | #154306 | 1/100 |
| Anti-Mouse Granzyme B FITC | QA16A02 | BioLegend | #372206 | 1/100 |
| Anti-Mouse IFN-γ Brilliant Violet 650™ | XMG1.2 | BioLegend | #505832 | 1/100 |

| Anti-Mouse IL-2 Brilliant Violet 711™ | JES6-5H4 | BioLegend | #503837 | 1/100 |
| Anti-Mouse T-bet Brilliant Violet 711™ | 4B10 | BioLegend | #644820 | 1/100 |
| Anti-Mouse ICOS PerCP-Cyanine5.5 | 7E.17G9 | BioLegend | #117424 | 1/200 |
| Anti-Mouse CD25 APC | PC61.5 | Thermo Fisher | #17-0251-82 | 1/200 |
| Anti-Mouse FoxP3 eFluor™ 450 | FJK-16s | Thermo Fisher | #48-5773-82 | 1/100 |
| Anti-Mouse HIF1α APC | Mgc3 | Thermo Fisher | #17-7528-82 | 1/100 |
| Anti-Mouse Ki-67 Alexa Fluor® 700 | SolA15 | Thermo Fisher | #56-5698-82 | 1/100 |
| Anti-Human/Mouse Glut1 Alexa Fluor® 405 | EPR3915 | Abcam | #ab210438 | 1/100 |
| Anti-Human CD3 Super Bright™ 702 | OKT3 | Thermo Fisher | #67-0037-42 | 1/200 |
| Anti-Human IFN-γ Brilliant Violet 605™ | B27 | BD Biosciences | #562974 | 1/100 |
| Anti-Human CD4 Brilliant Violet 650™ | L200 | BD Biosciences | #563737 | 1/200 |

719

## Western blot (WB)

720
721 Western blot was performed, as previously described[69]. Briefly, cells were washed with cold
722 DPBS twice before lysed with M-PER buffer (Thermo Scientific, #78501) containing proteinase
723 inhibitors cOmplete (Roche, #11836170001) and phosphatase inhibitors (Sigma, #P2850 and
724 P5726). Lysates were then collected and transferred to 1.5 mL Eppendorf tubes and sonicated.
725 Protein concentration was determined by NanoDrop. Fifty μg of total proteins were loaded onto
726 each lane of an 8-12% SDS-PAGE gel. After electrophoresis, proteins on the gel were
727 transferred to 0.45 μm of PVDF membrane (Millipore, #IPVH00005) in a sponge sandwich.
728 Membranes were then blocked with 5% of non-fat milk (Bio-Rad, #170-6404) and probed with
729 primary antibodies overnight on a shaker in cold room. Membranes were then washed and
730 incubated with HRP-conjugated secondary antibodies for 1 h at room temperature. The
731 membranes were then incubated with Western HRP substrate (Millipore, WBLUR0500) for 2-5
732 min before imaging with an X-ray film. The antibodies used for WB are listed in Supplemental
733 Table. β-actin was blot as loading control on the same gel with proteins of interest. Uncropped
734 and unprocessed scans of all blots were provided in the Source Data file.

| Name | Clone | Source | Catalog | Antibody dilution |
|---|---|---|---|---|
| HIF-1α | D2U3T | Santa Cruz Biotechnology | 14179S | 1/1000 |
| Glut1 | polyclonal | Sigma | 07-1401 | 1/1000 |
| Hk2 | C64G5 | Cell Signaling Technology | #2867 | 1/1000 |
| Ldha | Polyclonal | Cell Signaling Technology | 2012S | 1/1000 |
| Pkm2 | D78A4 | Cell Signaling Technology | 4053T | 1/1000 |
| Mct4 | D-1 | Santa Cruz Biotechnology | sc-376140 | 1/1000 |
| β-Actin | C-4 | Santa Cruz Biotechnology | sc-47778 HRP | 1/10000 |

735

## Acetyl-CoA measurement

736
737 Naïve CD4 T cells were differentiated under hypoxia for 4 days before cultured in fresh Click's
738 medium for another 24h with or without 20mM sodium acetate. Cells were lysed with M-PER
739 buffer for 10 minutes on ice. Cell lysates were spun down at 13000 rpm for 10min at 4 °C.
740 Supernatant was deproteinized using 4M perchloric acid and neutralized by 1N potassium
741 hydroxide. Then deproteinized lysates were used for acetyl-coA measurement using Acetyl-
742 Coenzyme A Assay Kit (Sigma, #MAK039) following the manufacturer's instructions.
743 Fluorescence intensity was measured at Ex/Em=535/587nM. Acetyl-coA levels were normalized
744 to cell number.

745
746

747 ***RT-PCR***
748 Total RNAs were extracted from cells using RNeasy Plus Mini kit (QIAGEN, #74136) according
749 to the manufacturer's instructions. Reverse transcription polymerase chain reaction (RT-PCR)
750 was done, as we previously described[48]. In brief, first-strand cDNAs were synthesized by
751 SuperScript III reverse transcriptase (Invitrogen, # 11752250) according to the manufacturer's
752 instructions. Up to 1µg of total RNA was used for reverse transcription. First-strand cDNA was
753 diluted 20 times for quantitative RT-PCR which was performed on Bio-Rad CFX96 instrument.
754 The primers are listed in Supplemental Table. β-actin was used as the housekeeping gene.
755 Specificity of primers were all validated by single peak of melting curve. The gene expression
756 level was calculated using the $2^{-\Delta\Delta CT}$ method.

| Gene name | Forward primer | Reverse primer |
|---|---|---|
| Hif1α | AGCTTCTGTTATGAGGCTCACC | TGACTTGATGTTCATCGTCCTC |
| Glut1 | CAGTTCGGCTATAACACTGGTG | GCCCCCGACAGAGAAGATG |
| Hk2 | TGATCGCCTGCTTATTCACGG | AACCGCCTAGAAATCTCCAGA |
| Gpi | TCAAGCTGCGCGAACTTTTTG | GGTTCTTGGAGTAGTCCACCAG |
| Tpi1 | CCAGGAAGTTCTTCGTTGGGG | CAAAGTCGATGTAAGCGGTGG |
| Pkm2 | GCCGCCTGGACATTGACTC | CCATGAGAGAAATTCAGCCGAG |
| Eno1 | TGCGTCCACTGGCATCTAC | CAGAGCAGGCGCAATAGTTTTA |
| Ldha | CATTGTCAAGTACAGTCCACACT | TTCCAATTACTCGGTTTTTGGGA |
| Mct4 | TCACGGGTTTCTCCTACGC | GCCAAAGCGGTTCACACAC |
| Actin | CATTGCTGACAGGATGCAGAAGG | TGCTGGAAGGTGGACAGTGAGG |

757
758 ***RNA-seq analysis***
759 Naïve CD4 T cells isolated from WT or HIF1α[CD4] mice were activated for 48h under hypoxia.
760 Cells were directly lysed on the plate and total RNA was extracted immediately by RNeasy Plus
761 Mini Kit from QIAGEN, Inc. Standard RNA-seq was performed by GENEWIZ, Inc. Briefly, total
762 RNA was enriched with Poly A selection and sequencing was performed on Illumina platform.
763 For RNA-seq data analysis, paired-end transcriptome sequences were mapped to the *Mus*
764 *musculus* GRCm38 reference genome available on ENSEMBL using the STAR aligner (version
765 2.7.5a. Read counts per gene were calculated using htseq-count in the HTseq package (version
766 0.11.2)[70]. Then the read counts per gene were used for downstream differential gene
767 expression analysis and pathway enrichment analysis. The analysis of differentially expressed
768 genes (DEGs) between WT control and HIF1α[−□] samples was performed using DESeq2
769 (version 1.34.0)[71] in R (version 3.6.0). The Wald test was used to calculate the p-values and
770 log2 fold changes. Genes with an adjusted p-value <0.05 and absolute log2 fold change >1
771 were considered as DEGs. A volcano plot was used to show all upregulated and downregulated
772 DEGs using the ggplot2 package (version 3.3.6) (ggplot2: Elegant Graphics for Data Analysis.
773 Springer-Verlag New York. ISBN 978-3-319-24277-4, https://ggplot2.tidyverse.org). Enriched
774 Kyoto Encyclopedia of Genes and Genomes (KEGG) pathways[72] of the DEGs were identified by
775 enrichr package[73] (version 3.0), a comprehensive gene set enrichment analysis tool. Significant
776 terms of the KEGG pathways were selected with a p-value <0.05.

777
778 ***Statistical analysis***
779 For animal experiments, 5-7 mice were included in each group; for *in vitro* studies with cells,
780 triplicates were set up to ensure consistency and reproducibility. All experiments were repeated
781 for 2-5 times. Representative results were expressed as mean ± SEM. Data were analyzed
782 using a two-sided Student's t-test, one-way ANOVA, or two-way ANOVA after confirming their
783 normal distribution. All analyses were performed using Prism 9.4.0 (GraphPad Software, Inc.)
784 and p < 0.05 was considered statistically significant.

809

810    **References**
811    1    Mosmann, T. R., Cherwinski, H., Bond, M. W., Giedlin, M. A. & Coffman, R. L. Two types
812         of murine helper T cell clone. I. Definition according to profiles of lymphokine activities
813         and secreted proteins. *J Immunol* **136**, 2348-2357 (1986).
814    2    Harrington, L. E. *et al.* Interleukin 17-producing CD4+ effector T cells develop via a
815         lineage distinct from the T helper type 1 and 2 lineages. *Nat Immunol* **6**, 1123-1132,
816         doi:10.1038/ni1254 (2005).
817    3    Sakaguchi, S., Sakaguchi, N., Asano, M., Itoh, M. & Toda, M. Immunologic self-
818         tolerance maintained by activated T cells expressing IL-2 receptor alpha-chains (CD25).
819         Breakdown of a single mechanism of self-tolerance causes various autoimmune
820         diseases. *J Immunol* **155**, 1151-1164 (1995).
821    4    Shen, H. & Shi, L. Z. Metabolic regulation of TH17 cells. *Mol Immunol* **109**, 81-87,
822         doi:10.1016/j.molimm.2019.03.005 (2019).
823    5    Chang, C. H. *et al.* Posttranscriptional control of T cell effector function by aerobic
824         glycolysis. *Cell* **153**, 1239-1251, doi:10.1016/j.cell.2013.05.016 (2013).
825    6    Ho, P. C. *et al.* Phosphoenolpyruvate Is a Metabolic Checkpoint of Anti-tumor T Cell
826         Responses. *Cell* **162**, 1217-1228, doi:10.1016/j.cell.2015.08.012 (2015).
827    7    Michalek, R. D. *et al.* Cutting edge: distinct glycolytic and lipid oxidative metabolic
828         programs are essential for effector and regulatory CD4+ T cell subsets. *J Immunol* **186**,
829         3299-3303, doi:10.4049/jimmunol.1003613 (2011).
830    8    Shi, L. Z. *et al.* HIF1alpha-dependent glycolytic pathway orchestrates a metabolic
831         checkpoint for the differentiation of TH17 and Treg cells. *J Exp Med* **208**, 1367-1376,
832         doi:10.1084/jem.20110278 (2011).
833    9    Wang, R. *et al.* The transcription factor Myc controls metabolic reprogramming upon T
834         lymphocyte activation. *Immunity* **35**, 871-882, doi:10.1016/j.immuni.2011.09.021 (2011).

835 10 Pearce, E. L. *et al.* Enhancing CD8 T-cell memory by modulating fatty acid metabolism.
836 *Nature* **460**, 103-107, doi:10.1038/nature08097 (2009).
837 11 van der Windt, G. J. *et al.* Mitochondrial respiratory capacity is a critical regulator of
838 CD8+ T cell memory development. *Immunity* **36**, 68-78,
839 doi:10.1016/j.immuni.2011.12.007 (2012).
840 12 Ma, E. H. *et al.* Serine Is an Essential Metabolite for Effector T Cell Expansion. *Cell*
841 *metabolism* **25**, 482, doi:10.1016/j.cmet.2017.01.014 (2017).
842 13 Mondanelli, G. *et al.* A Relay Pathway between Arginine and Tryptophan Metabolism
843 Confers Immunosuppressive Properties on Dendritic Cells. *Immunity* **46**, 233-244,
844 doi:10.1016/j.immuni.2017.01.005 (2017).
845 14 Hu, X. *et al.* Synthetic RORgamma agonists regulate multiple pathways to enhance
846 antitumor immunity. *Oncoimmunology* **5**, e1254854,
847 doi:10.1080/2162402X.2016.1254854 (2016).
848 15 Bensinger, S. J. *et al.* LXR signaling couples sterol metabolism to proliferation in the
849 acquired immune response. *Cell* **134**, 97-111, doi:10.1016/j.cell.2008.04.052 (2008).
850 16 Pearce, E. L. Metabolism in T cell activation and differentiation. *Curr Opin Immunol* **22**,
851 314-320, doi:10.1016/j.coi.2010.01.018 (2010).
852 17 Chi, H. Regulation and function of mTOR signalling in T cell fate decisions. *Nat Rev*
853 *Immunol* **12**, 325-338, doi:10.1038/nri3198 (2012).
854 18 Zenewicz, L. A. Oxygen Levels and Immunological Studies. *Front Immunol* **8**, 324,
855 doi:10.3389/fimmu.2017.00324 (2017).
856 19 Habler, O. P. & Messmer, K. F. The physiology of oxygen transport. *Transfus Sci* **18**,
857 425-435, doi:10.1016/s0955-3886(97)00041-6 (1997).
858 20 Caldwell, C. C. *et al.* Differential effects of physiologically relevant hypoxic conditions on
859 T lymphocyte development and effector functions. *J Immunol* **167**, 6140-6149,
860 doi:10.4049/jimmunol.167.11.6140 (2001).
861 21 Cho, S. H. *et al.* Germinal centre hypoxia and regulation of antibody qualities by a
862 hypoxia response system. *Nature* **537**, 234-238, doi:10.1038/nature19334 (2016).
863 22 Brandtzaeg, P. *et al.* Immunobiology and immunopathology of human gut mucosa:
864 humoral immunity and intraepithelial lymphocytes. *Gastroenterology* **97**, 1562-1584,
865 doi:10.1016/0016-5085(89)90406-x (1989).
866 23 Karhausen, J. *et al.* Epithelial hypoxia-inducible factor-1 is protective in murine
867 experimental colitis. *J Clin Invest* **114**, 1098-1106, doi:10.1172/jci21086 (2004).
868 24 Carreau, A., El Hafny-Rahbi, B., Matejuk, A., Grillon, C. & Kieda, C. Why is the partial
869 oxygen pressure of human tissues a crucial parameter? Small molecules and hypoxia. *J*
870 *Cell Mol Med* **15**, 1239-1253, doi:10.1111/j.1582-4934.2011.01258.x (2011).
871 25 Palazon, A., Aragones, J., Morales-Kastresana, A., de Landazuri, M. O. & Melero, I.
872 Molecular pathways: hypoxia response in immune cells fighting or promoting cancer.
873 *Clin Cancer Res* **18**, 1207-1213, doi:10.1158/1078-0432.CCR-11-1591 (2012).
874 26 Colgan, S. P. & Taylor, C. T. Hypoxia: an alarm signal during intestinal inflammation. *Nat*
875 *Rev Gastroenterol Hepatol* **7**, 281-287, doi:10.1038/nrgastro.2010.39 (2010).
876 27 Semenza, G. L. Targeting HIF-1 for cancer therapy. *Nat Rev Cancer* **3**, 721-732,
877 doi:10.1038/nrc1187 (2003).
878 28 Maxwell, P. H. *et al.* The tumour suppressor protein VHL targets hypoxia-inducible
879 factors for oxygen-dependent proteolysis. *Nature* **399**, 271-275, doi:10.1038/20459
880 (1999).
881 29 Tanimoto, K., Makino, Y., Pereira, T. & Poellinger, L. Mechanism of regulation of the
882 hypoxia-inducible factor-1 alpha by the von Hippel-Lindau tumor suppressor protein.
883 *Embo j* **19**, 4298-4309, doi:10.1093/emboj/19.16.4298 (2000).

884   30   Lando, D., Peet, D. J., Whelan, D. A., Gorman, J. J. & Whitelaw, M. L. Asparagine
885        hydroxylation of the HIF transactivation domain a hypoxic switch. *Science* **295**, 858-861,
886        doi:10.1126/science.1068592 (2002).

887   31   Zhu, J. & Paul, W. E. CD4 T cells: fates, functions, and faults. *Blood* **112**, 1557-1569,
888        doi:10.1182/blood-2008-05-078154 (2008).

889   32   Bollinger, T. *et al.* HIF-1alpha- and hypoxia-dependent immune responses in human
890        CD4+CD25high T cells and T helper 17 cells. *Journal of leukocyte biology* **96**, 305-312,
891        doi:10.1189/jlb.3A0813-426RR (2014).

892   33   Shehade, H., Acolty, V., Moser, M. & Oldenhove, G. Cutting Edge: Hypoxia-Inducible
893        Factor 1 Negatively Regulates Th1 Function. *J Immunol* **195**, 1372-1376,
894        doi:10.4049/jimmunol.1402552 (2015).

895   34   Marusina, A. I. *et al.* CD4(+) virtual memory: Antigen-inexperienced T cells reside in the
896        naïve, regulatory, and memory T cell compartments at similar frequencies, implications
897        for autoimmunity. *Journal of autoimmunity* **77**, 76-88, doi:10.1016/j.jaut.2016.11.001
898        (2017).

899   35   Beyer, M. & Schultze, J. L. CD4+CD25highFOXP3+ regulatory T cells in peripheral
900        blood are primarily of effector memory phenotype. *Journal of clinical oncology : official
901        journal of the American Society of Clinical Oncology* **25**, 2628-2630; author reply 2630-
902        2622, doi:10.1200/jco.2006.08.0192 (2007).

903   36   Peng, M. *et al.* Aerobic glycolysis promotes T helper 1 cell differentiation through an
904        epigenetic mechanism. *Science* **354**, 481-484, doi:10.1126/science.aaf6284 (2016).

905   37   Cho, S. H. *et al.* Hypoxia-inducible factors in CD4(+) T cells promote metabolism, switch
906        cytokine secretion, and T cell help in humoral immunity. *Proc Natl Acad Sci U S A* **116**,
907        8975-8984, doi:10.1073/pnas.1811702116 (2019).

908   38   Coyle, A. J. *et al.* The CD28-related molecule ICOS is required for effective T cell-
909        dependent immune responses. *Immunity* **13**, 95-105 (2000).

910   39   Lee, J. H., Elly, C., Park, Y. & Liu, Y. C. E3 Ubiquitin Ligase VHL Regulates Hypoxia-
911        Inducible Factor-1α to Maintain Regulatory T Cell Stability and Suppressive Capacity.
912        *Immunity* **42**, 1062-1074, doi:10.1016/j.immuni.2015.05.016 (2015).

913   40   Moussaieff, A. *et al.* Glycolysis-mediated changes in acetyl-CoA and histone acetylation
914        control the early differentiation of embryonic stem cells. *Cell metabolism* **21**, 392-402,
915        doi:10.1016/j.cmet.2015.02.002 (2015).

916   41   Shi, L. Z. *et al.* Interdependent IL-7 and IFN-gamma signalling in T-cell controls tumour
917        eradication by combined alpha-CTLA-4+alpha-PD-1 therapy. *Nat Commun* **7**, 12335,
918        doi:10.1038/ncomms12335 (2016).

919   42   Fu, T., He, Q. & Sharma, P. The ICOS/ICOSL pathway is required for optimal antitumor
920        responses mediated by anti-CTLA-4 therapy. *Cancer Res* **71**, 5445-5454, doi:0008-
921        5472.CAN-11-1138 [pii] (2011).

922   43   Curran, M. A., Montalvo, W., Yagita, H. & Allison, J. P. PD-1 and CTLA-4 combination
923        blockade expands infiltrating T cells and reduces regulatory T and myeloid cells within
924        B16 melanoma tumors. *Proc Natl Acad Sci U S A* **107**, 4275-4280,
925        doi:10.1073/pnas.0915174107 (2010).

926   44   Yang, K. *et al.* T cell exit from quiescence and differentiation into Th2 cells depend on
927        Raptor-mTORC1-mediated metabolic reprogramming. *Immunity* **39**, 1043-1056,
928        doi:10.1016/j.immuni.2013.09.015 (2013).

929   45   Setoguchi, R., Matsui, Y. & Mouri, K. mTOR signaling promotes a robust and continuous
930        production of IFN-γ by human memory CD8+ T cells and their proliferation. *Eur J
931        Immunol* **45**, 893-902, doi:10.1002/eji.201445086 (2015).

932   46   Nagata, S. Human autoimmune lymphoproliferative syndrome, a defect in the apoptosis-
933        inducing Fas receptor: a lesson from the mouse model. *J Hum Genet* **43**, 2-8,
934        doi:10.1007/s100380050029 (1998).

935 47    Wells, A. D. *et al.* Requirement for T-cell apoptosis in the induction of peripheral
936        transplantation tolerance. *Nat Med* **5**, 1303-1307, doi:10.1038/15260 (1999).
937 48    Shi, L. Z. *et al.* Inhibitory role of the transcription repressor Gfi1 in the generation of
938        thymus-derived regulatory T cells. *Proc Natl Acad Sci U S A* **110**, E3198-3205,
939        doi:10.1073/pnas.1300950110 (2013).
940 49    Refaeli, Y., Van Parijs, L., Alexander, S. I. & Abbas, A. K. Interferon gamma is required
941        for activation-induced death of T lymphocytes. *J Exp Med* **196**, 999-1005,
942        doi:10.1084/jem.20020666 (2002).
943 50    Shen, H. *et al.* Predictive biomarkers for immune checkpoint blockade and opportunities
944        for combination therapies. *Genes & Diseases* (2019).
945 51    Cella, D. *et al.* Patient-reported outcomes of patients with advanced renal cell carcinoma
946        treated with nivolumab plus ipilimumab versus sunitinib (CheckMate 214): a randomised,
947        phase 3 trial. *The lancet oncology* **20**, 297-310, doi:10.1016/S1470-2045(18)30778-2
948        (2019).
949 52    Antonia, S. J. *et al.* Durvalumab after Chemoradiotherapy in Stage III Non-Small-Cell
950        Lung Cancer. *N Engl J Med* **377**, 1919-1929, doi:10.1056/NEJMoa1709937 (2017).
951 53    Socinski, M. A. *et al.* Atezolizumab for First-Line Treatment of Metastatic Nonsquamous
952        NSCLC. *N Engl J Med* **378**, 2288-2301, doi:10.1056/NEJMoa1716948 (2018).
953 54    Gandhi, L. *et al.* Pembrolizumab plus Chemotherapy in Metastatic Non-Small-Cell Lung
954        Cancer. *N Engl J Med* **378**, 2078-2092, doi:10.1056/NEJMoa1801005 (2018).
955 55    Wolchok, J. D. *et al.* Overall Survival with Combined Nivolumab and Ipilimumab in
956        Advanced Melanoma. *N Engl J Med* **377**, 1345-1356, doi:10.1056/NEJMoa1709684
957        (2017).
958 56    Peggs, K. S., Quezada, S. A., Korman, A. J. & Allison, J. P. Principles and use of anti-
959        CTLA4 antibody in human cancer immunotherapy. *Curr Opin Immunol* **18**, 206-213,
960        doi:10.1016/j.coi.2006.01.011 (2006).
961 57    Wolchok, J. D. *et al.* Long-Term Outcomes With Nivolumab Plus Ipilimumab or
962        Nivolumab Alone Versus Ipilimumab in Patients With Advanced Melanoma. *Journal of
963        clinical oncology : official journal of the American Society of Clinical Oncology* **40**, 127-
964        137, doi:10.1200/JCO.21.02229 (2022).
965 58    Palazon, A. *et al.* An HIF-1alpha/VEGF-A Axis in Cytotoxic T Cells Regulates Tumor
966        Progression. *Cancer Cell* **32**, 669-683 e665, doi:10.1016/j.ccell.2017.10.003 (2017).
967 59    Sharma, P., Hu-Lieskovan, S., Wargo, J. A. & Ribas, A. Primary, Adaptive, and Acquired
968        Resistance to Cancer Immunotherapy. *Cell* **168**, 707-723, doi:10.1016/j.cell.2017.01.017
969        (2017).
970 60    Lee, J. H., Elly, C., Park, Y. & Liu, Y. C. E3 Ubiquitin Ligase VHL Regulates Hypoxia-
971        Inducible Factor-1alpha to Maintain Regulatory T Cell Stability and Suppressive
972        Capacity. *Immunity* **42**, 1062-1074, doi:10.1016/j.immuni.2015.05.016 (2015).
973 61    Doedens, A. L. *et al.* Hypoxia-inducible factors enhance the effector responses of
974        CD8(+) T cells to persistent antigen. *Nat Immunol* **14**, 1173-1182, doi:10.1038/ni.2714
975        (2013).
976 62    Bisilliat Donnet, C. *et al.* PHD2 Constrains Antitumor CD8+ T-cell Activity. *Cancer
977        immunology research* **11**, 339-350, doi:10.1158/2326-6066.Cir-22-0099 (2023).
978 63    Gropper, Y. *et al.* Culturing CTLs under Hypoxic Conditions Enhances Their Cytolysis
979        and Improves Their Anti-tumor Function. *Cell Rep* **20**, 2547-2555,
980        doi:10.1016/j.celrep.2017.08.071 (2017).
981 64    Chang, C. H. *et al.* Metabolic Competition in the Tumor Microenvironment Is a Driver of
982        Cancer Progression. *Cell* **162**, 1229-1241, doi:10.1016/j.cell.2015.08.016 (2015).
983 65    Zappasodi, R. *et al.* CTLA-4 blockade drives loss of Treg stability in glycolysis-low
984        tumours. *Nature*, doi:10.1038/s41586-021-03326-4 (2021).

985   66   Li, W., Cheng, H., Li, G. & Zhang, L. Mitochondrial Damage and the Road to Exhaustion.
986        *Cell metabolism* **32**, 905-907, doi:10.1016/j.cmet.2020.11.004 (2020).
987   67   Shi, L. Z. *et al.* Gfi1-Foxo1 axis controls the fidelity of effector gene expression and
988        developmental maturation of thymocytes. *Proc Natl Acad Sci U S A* **114**, E67-E74,
989        doi:10.1073/pnas.1617669114 (2017).
990   68   Shen, H. *et al.* Selective suppression of melanoma lacking IFN-γ pathway by JAK
991        inhibition depends on T cells and host TNF signaling. *Nat Commun* **13**, 5013,
992        doi:10.1038/s41467-022-32754-7 (2022).
993   69   Shen, H. *et al.* MicroRNA-30a attenuates mutant KRAS-driven colorectal tumorigenesis
994        via direct suppression of ME1. *Cell Death Differ* **24**, 1253-1262,
995        doi:10.1038/cdd.2017.63 (2017).
996   70   Anders, S., Pyl, P. T. & Huber, W. HTSeq--a Python framework to work with high-
997        throughput sequencing data. *Bioinformatics* **31**, 166-169,
998        doi:10.1093/bioinformatics/btu638 (2015).
999   71   Love, M. I., Huber, W. & Anders, S. Moderated estimation of fold change and dispersion
1000       for RNA-seq data with DESeq2. *Genome Biol* **15**, 550, doi:10.1186/s13059-014-0550-8
1001       (2014).
1002  72   Kanehisa, M., Furumichi, M., Tanabe, M., Sato, Y. & Morishima, K. KEGG: new
1003       perspectives on genomes, pathways, diseases and drugs. *Nucleic Acids Res* **45**, D353-
1004       d361, doi:10.1093/nar/gkw1092 (2017).
1005  73   Kuleshov, M. V. *et al.* Enrichr: a comprehensive gene set enrichment analysis web
1006       server 2016 update. *Nucleic Acids Res* **44**, W90-97, doi:10.1093/nar/gkw377 (2016).
1007

**Figure 1**
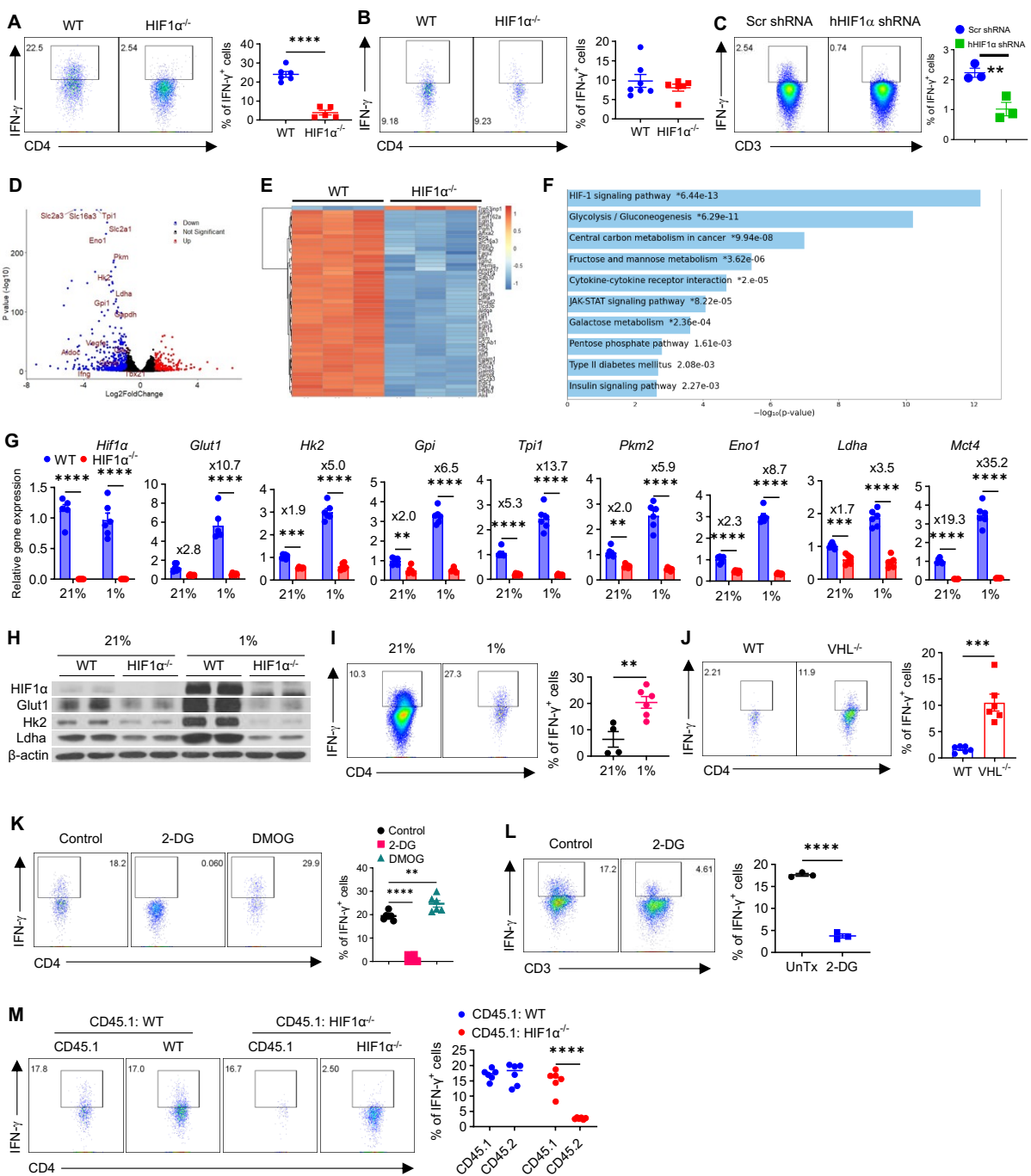
**Figure 1. HIF1α-glycolysis controls IFN-γ induction in hypoxic T cells, *in vitro*. A-B**. Naïve CD4+ T cells isolated from WT and HIF1α⁻/⁻ mice were activated under hypoxia (**A**) and normoxia (**B**) for 5.5 days, followed by detection of IFN-γ. **C**. Naive human CD4 T cells isolated from PBMCs of healthy donors were activated, transduced with retroviruses expressing scrambled shRNAs (Scr shRNA) or shRNAs against human HIF1α (hHIF1α shRNA), and cultured under hypoxia for 5.5 days, followed by detection of IFN-γ. **D-F**. Total RNAs extracted from WT and HIF1α⁻/⁻ CD4 naïve T cells activated under hypoxia for 48h were subjected to RNA-Seq. The gene expression analyses were performed using DESeq2 (version 1.34.0). The Wald test was used to calculate the p values and log2 fold changes. Genes with an adjusted p value < 0.05 and absolute log2 fold change > 1 were considered as differentially expressed genes (DEGs). A volcano plot was used to show all upregulated and downregulated DEGs using the ggplot2 R packagew (**D**), with top 50 identified DEGs shown as a heatmap (**E**). Top 10 enriched signaling pathways (downregulated) from Enriched Kyoto Encyclopedia of Genes and Genomes (KEGG) analyses of DEGs were shown in **F**. Significant terms of the KEGG pathways were selected with p value <0.05. **G**. mRNA expression of glycolytic genes was evaluated by real-time RT-PCR in T cells activated and cultured under normoxia (21%) and hypoxia (1%) for 48h. **H**. Protein expression of HIF1α, Glut1, Hk2, and Ldha was analyzed using cell lysates prepared using cells similarly activated as in **G**; β-actin was used as a loading control. **I.** WT naïve CD4 T cells were similarly activated under normoxia and hypoxia as in **A** for 5.5 days and analyzed for IFN-γ production. **J**. IFN-γ production by WT or VHL⁻/⁻ CD4 T cells activated under hypoxia for 2.5 days. **K**. Naïve WT CD4 T cells were similarly activated under hypoxia, in the presence of solvent (Control), 0.5 μM of 2-DG, or 0.2μM of DMOG, for 5.5 days, followed by analysis of IFN-γ production. L. Naive human CD4 T cells isolated from PBMCs of healthy donors were activated under hypoxia for 5.5 days, with or without 0.5 μM 2-DG, followed by detection of IFN-γ. **M**. Equally mixed naïve CD45.1 CD4 T cells with naïve CD45.2 CD4 T cells from WT or HIF1α⁻/⁻ mice were activated under hypoxia for 5.5 days and detected for IFN-γ production. All the experiments were repeated at least twice. Pooled results shown in the dot plots and bar graphs depicted means ± SEM for all samples in each group, with each dot denoting an independent sample. **, p<0.01; ***, p<0.001; ****, p<0.0001. Source data were provided in the Source Data file.
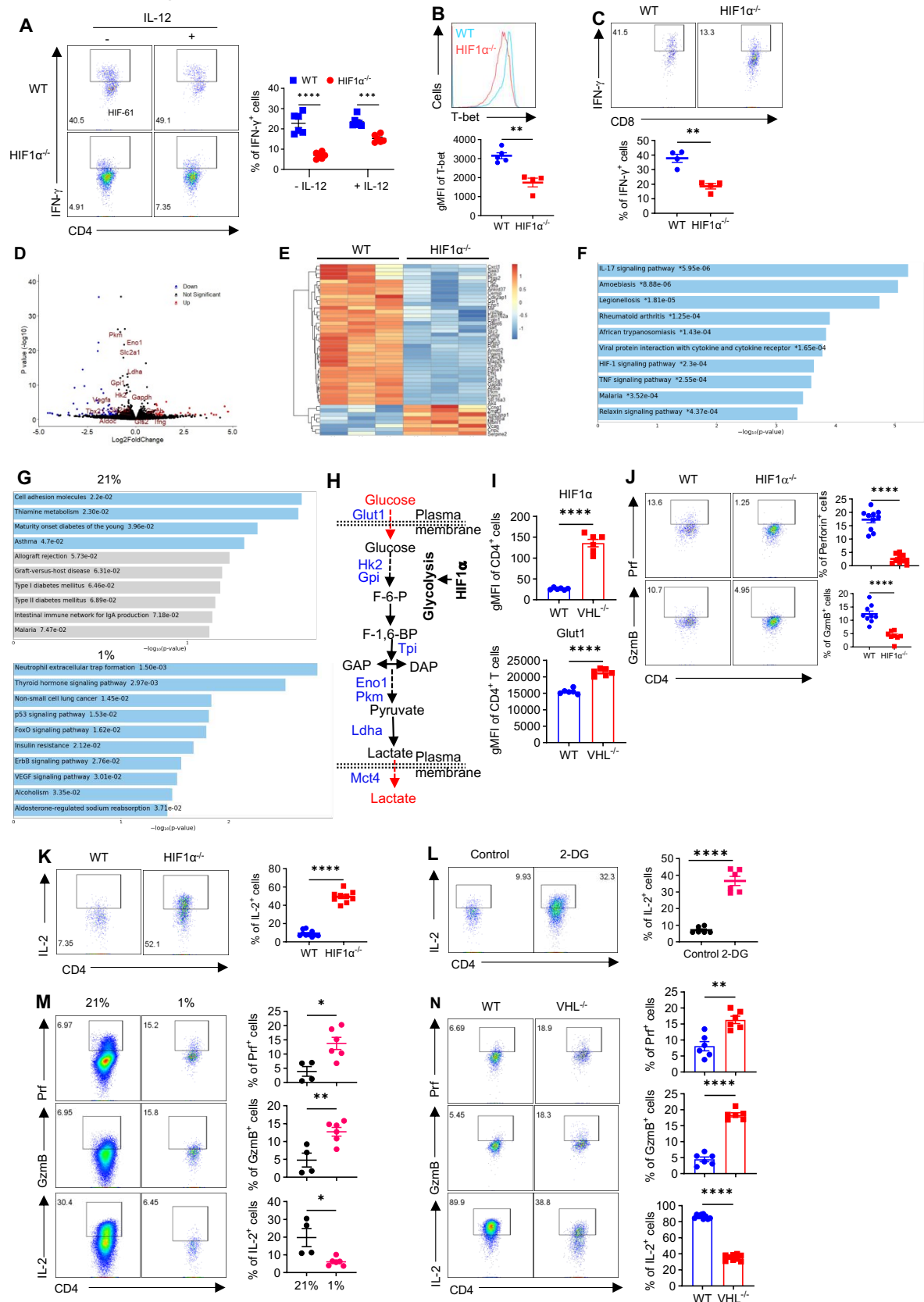
**Supplemental Figure 1**

1040 **Figure S1. HIF1$\alpha$-glycolysis controls IFN-γ induction in hypoxic T cells, *in vitro*. A**. Naïve
1041 CD4$^\square$ T cells isolated from WT and HIF1$\alpha^{-/-}$ mice were activated under hypoxia for 5.5 days,
1042 with or without IL-12, followed by IFN-$\gamma$ detection of . **B**. T-bet expression in WT and HIF1$\alpha^{-/-}$
1043 CD4$^\square$ T cells, activated under hypoxia for 2 days. **C**. Naïve CD8$^\square$ T cells from WT and HIF1$\alpha^{-/-}$
1044 mice were activated under hypoxia for 5.5 days and analyzed for IFN-$\gamma$ production. **D-G**. Total
1045 RNAs extracted from WT and HIF1$\alpha^{-/-}$ CD4$^\square$ T cells activated under normoxia for 48h were
1046 subjected to RNA-Seq. The gene expression analyses were performed using DESeq2 (version
1047 1.34.0). The Wald test was used to calculate the p values and log2 fold changes. Genes with an
1048 adjusted p value <0.05 and absolute log2 fold change > 1 were considered as differentially
1049 expressed genes (DEGs). A volcano plot was used to show all upregulated and downregulated
1050 DEGs using the ggplot2 R package (**D**), with top 50 identified DEGs shown in a heatmap (**E**).
1051 Top 10 enriched signaling pathways (downregulated) from Enriched Kyoto Encyclopedia of
1052 Genes and Genomes (KEGG) analyses of DEGs were shown in **F**. Significant terms of the
1053 KEGG pathways were selected with a p value <0.05. **G**. Significantly upregulated top 10
1054 enriched signaling pathways in HIF1$\alpha^{-/-}$ CD4$^\square$ T cells activated under normoxia (21% O$_2$)
1055 (Upper Panel) and hypoxia (1% O$_2$) (Lower Panel). **H.** A diagram of the glycolytic pathway, with
1056 the major glycolytic genes highlighted in blue. **I**. Geometric mean fluorescence intensity (gMFI)
1057 of HIF1$\alpha$ (Top) and Glut1 (Bottom) in WT or VHL$^{-/-}$ CD4$^\square$ T cells activated under hypoxia as in
1058 **A**. **J**. Production of perforin (Prf) and granzyme B (GzmB) by HIF1$\alpha^{-/-}$ CD4$^\square$ T cells in hypoxia
1059 for 5.5 days. **K**. IL-2 production by activated WT and HIF1$\alpha^{-/-}$ CD4$^\square$ T cells T cells activated in
1060 hypoxia for 5.5 days. **L**. IL-2 production by WT CD4$^\square$ T cells activated under hypoxia for 5.5
1061 days, treated with solvent (Control) or 0.5 µM of 2-DG. **M**. Production of Prf, GzmB, and IL-2 by
1062 CD4$^\square$ T cells activated under normoxia (21% O$_2$) and hypoxia (1% O$_2$) for 5.5 days. **N.**
1063 Production of Prf, GzmB, and IL-2 by WT or VHL$^{-/-}$ CD4$^\square$ T cells activated under hypoxia for 5.5
1064 days. All the experiments were repeated at least twice. Pooled results shown in the dot plots
1065 and bar graphs depicted means ± SEM for all samples in each group, with each dot denoting an
1066 independent sample. *, p<0.05; **, p<0.01; ***, p<0.001; ****, p<0.0001. Source data were
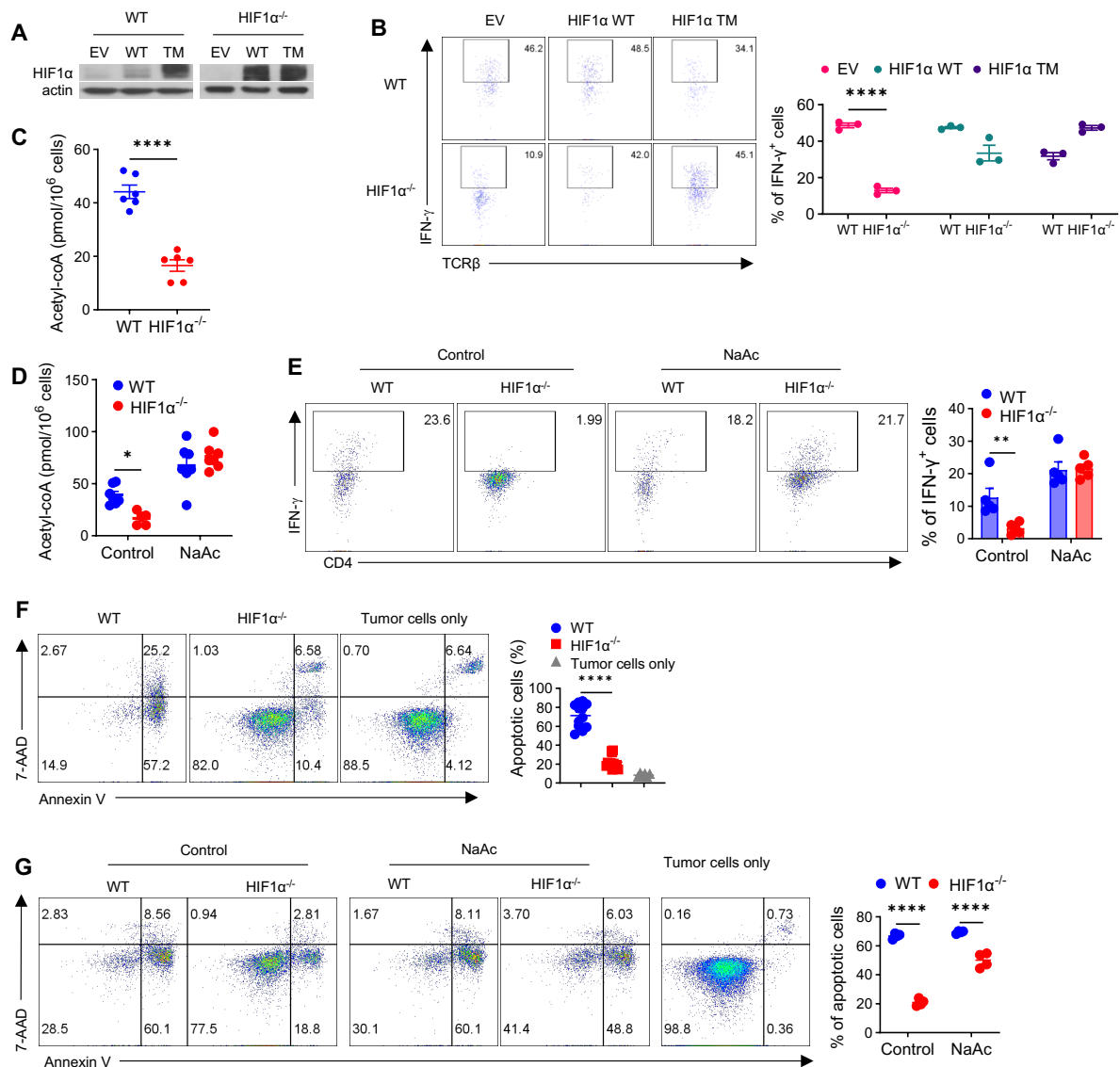1067 provided in the Source Data file.

**Figure 2**



1068

**Figure 2. Direct regulation of IFN-γ induction in hypoxic T cells by HIF1α and [acetyl-CoA], *in vitro*. A-B.** Protein expression of HIF1α in WT and HIF1α⁻/⁻ CD4⁺ T cells successfully transduced (GFP⁺) with empty retroviruses (EV) or retroviruses expressing WT or triple-mutant *Hif1a* (TM) (A). GFP⁺ T cells were activated under hypoxia and analyzed for IFN-γ production (**B**). **C.** [Acetyl-CoA] in activated WT and HIF1α⁻/⁻ CD4⁺ T cells. **D-E.** [Acetyl-CoA] (**D**) and IFN-γ production (**E**) by activated WT and HIF1α⁻/⁻ CD4⁺ T cells, with or without 20 mM sodium acetate (NaAc) added on Day 2 post-activation. **F.** Cell death of MB49 cells cultured alone (tumor cells only) or with activated WT and HIF1α⁻/⁻ CD4⁺ T cells at the ratio of 1:2 for 48h was measured by 7-AAD/Annexin V staining. **G.** Cell death of MB49 cells co-cultured with activated WT and HIF1α⁻/⁻ CD4⁺ T cells pretreated with or without NaAc for 48h was analyzed by 7-AAD/Annexin V staining. All experiments were repeated at least twice. Pooled results shown in the dot/bar graphs depicted means ± SEM for all the samples in each group, with each dot denoting an independent sample. **, p<0.01; ****, p<0.0001. Source data were provided in the Source Data file.

28

**Supplemental Figure 2.**
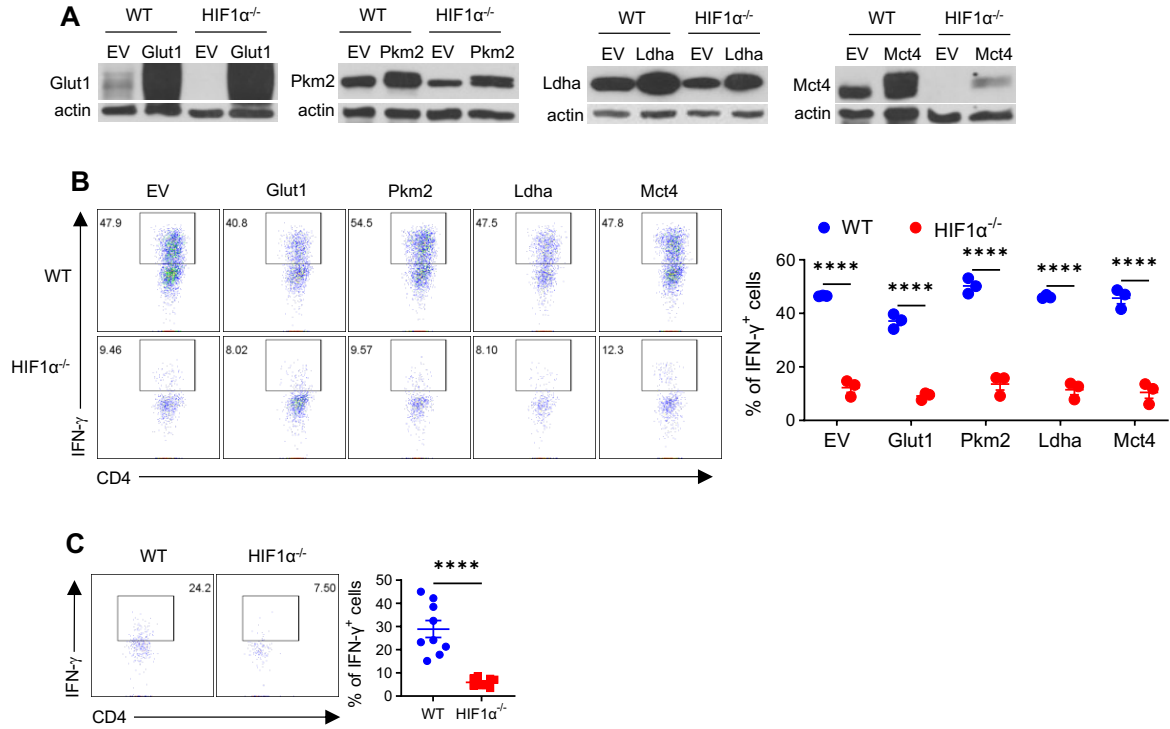


1083
**Figure S2. Direct regulation of IFN-γ induction in hypoxic T cells by HIF1α and intracellular acetyl CoA, *in vitro*. A.** Protein expression of Glut1, Pkm2, Ldha and Mct4 in activated WT and HIF1α$^{-/-}$ CD4 T cells successfully transduced (GFP ) with empty retroviruses (EV) or retroviruses expressing *Glut1*, *Pkm2*, *Ldha,* and *Mct4*, respectively. **B.** GFP T cells from **A** were activated under hypoxia for 5.5 days and analyzed for IFN-γ production. **C.** IFN-γ production by activated WT and HIF1α$^{-/-}$ CD4 T cells co-cultured with MB49 cells for 48h, under hypoxia. All the experiments were repeated at least twice. Pooled results shown in the dot plots depicted means ± SEM for all the samples in each group, with each dot denoting an independent sample. ****, p<0.0001. Source data were provided in the Source Data file.

**Figure 3**



1093
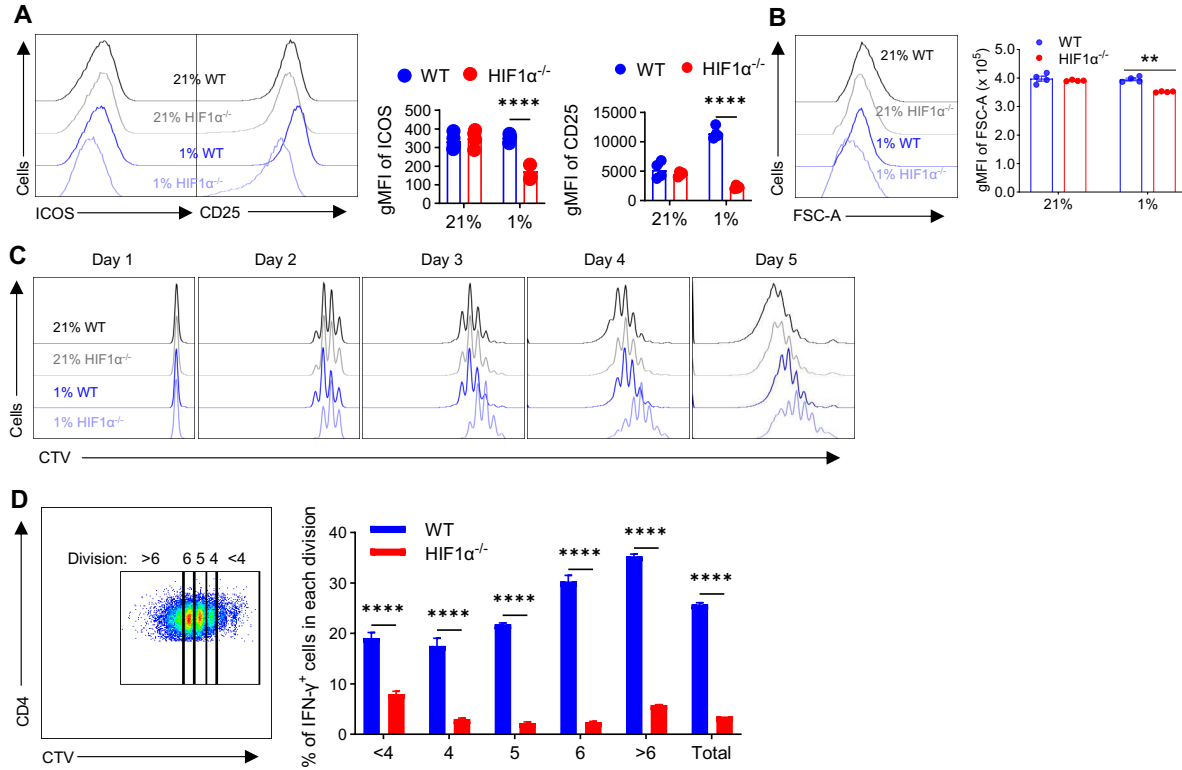
**Figure 3. Reduced IFN-γ production in HIF1α$^{-/-}$ T cells is not due to proliferative defect.**
**A-B**. Naïve WT and HIF1α$^{-/-}$ CD4 T cells were activated under normoxia (21% O$_2$) and hypoxia
(1% O$_2$) for 5.5 days. Gated live cells were analyzed for the expression of ICOS and CD25 (**A**),
depicted as geometric mean fluorescence intensity (gMFI), and area of forward scatter (FSC)
(**B**). **C-D**. Naïve WT and HIF1α$^{-/-}$ CD4 T cells were labeled with CellTrace Violet (CTV) and
activated under normoxia (21% O$_2$) and hypoxia (1% O$_2$). CTV dilution was monitored daily to
assess cell proliferation. Gating strategy on defining cell division by CTV dilution was shown for
WT T cells (left) and IFN-γ production by activated WT and HIF1α$^{-/-}$ CD4 T cells within
indicated cell divisions was shown by the bar graph on the right (**D**). All the experiments were
repeated at least twice. Pooled results shown in the dot plots and bar graphs depicted means ±
SEM for all the samples in each group, with each dot denoting an independent sample. **,
p<0.01; ****, p<0.0001. Source data were provided in the Source Data file.

**Supplemental Figure 3**
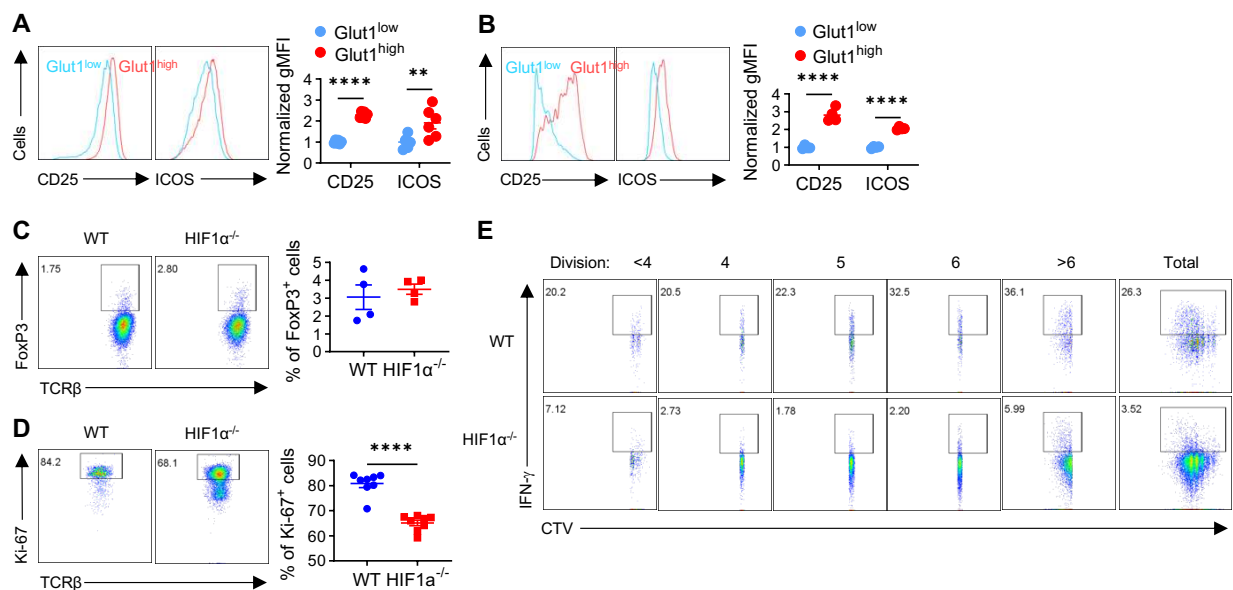


1106
1107 **Figure S3. Reduced IFN-γ production by HIF1α$^{-/-}$ T cells is not due to proliferative defect.**
1108 **A-B**. Naïve WT CD4$^{\square}$ (**A**) and CD8$^{\square}$ (**B**) T cells were activated under hypoxia for 2.5 days.
1109 Gated live Glut1$^{low}$ and Glut1$^{high}$ T cells were analyzed for the expression of ICOS and CD25,
1110 with geometric mean fluorescence intensity (gMFIs) shown in the dot scatter plot. **C-D**. Naïve
1111 WT and HIF1α$^{-/-}$ CD4$^{\square}$ T cells activated for 5.5 days under hypoxia were analyzed for FoxP3
1112 (**C**) and Ki-67 (**D**). **E**. CTV-labeled naïve WT and HIF1α$^{-/-}$ CD4$^{\square}$ T cells were activated under
1113 hypoxia. CTV dilution and IFN-γ production were detected on Day 5.5 following activation. All
1114 the experiments were repeated at least twice. Pooled results shown in the dot plots depicted
1115 means ± SEM for all the samples in each group, with each dot denoting an independent sample.
1116 **, p<0.01; ****, p<0.0001. Source data were provided in the Source Data file.

31
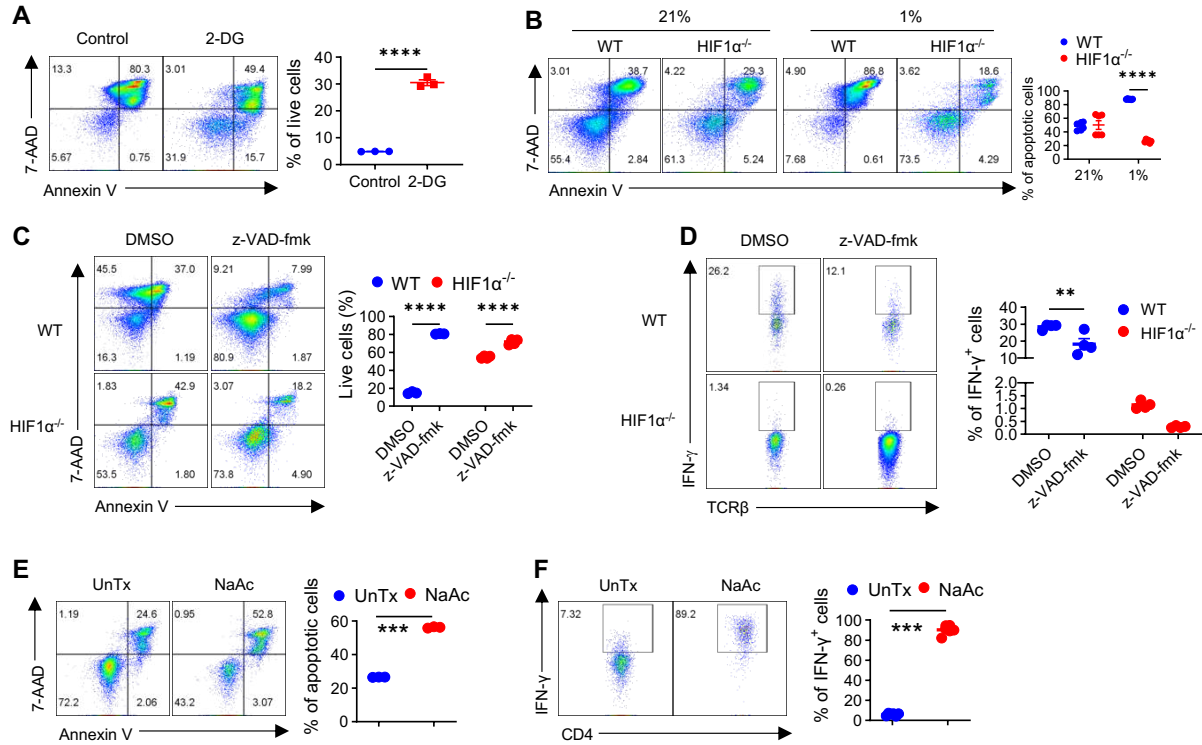
**Figure 4**



**Figure 4. HIF1α-glycolysis-driven AICD governs IFN-γ production in hypoxic T cells. A.**
Cell death of naïve WT CD4□ T cells activated under hypoxia for 3 days, with or without with 2-
DG was measured by 7-AAD/Annexin V staining. **B**. Cell death of naïve WT and HIF1α−/− CD4□
T cells activated under normoxia (21% $O_2$) and hypoxia (1% $O_2$) for 3 days was detected by 7-
AAD/Annexin V staining. **C-D**. Naïve WT and HIF1α−/− CD4□ T cells were activated under
hypoxia, with z-VAD-fmk or without (DMSO); on day 3, cells were stained for 7-AAD/Annexin V
to assess cell death (**C**), and on day 5, IFN-γ production was determined (**D**). **E-F**. Naïve
HIF1α−/− CD4□ T cells were activated under hypoxia, with or without 20mM sodium acetate
(NaAc) added on day 0; on day 3, cells were stained for7-AAD and Annexin V to assess cell
death (**E**), and IFN-γ production was determined on day 5 (**F**). All the experiments were
repeated at least twice. Pooled results shown in the dot plots depicted means ± SEM for all the
samples in each group, with each dot denoting an independent sample. **, p<0.01; ***, p<0.001;
****, p<0.0001. Source data were provided in the Source Data file.
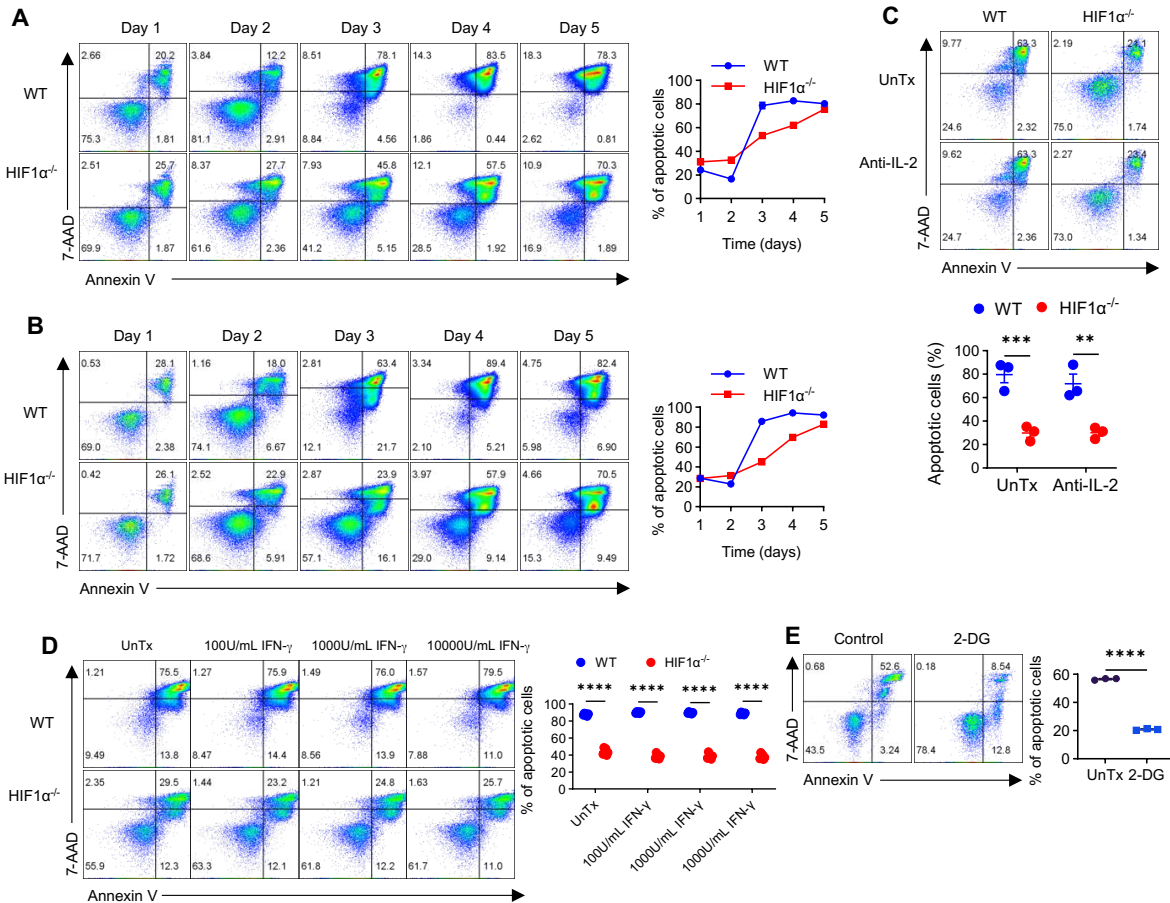
32

**Supplemental Figure 4**



1131

**Figure S4. Attenuated AICD in HIF1α$^{-/-}$ T cells is unlikely mediated by extrinsic factors. A**.
Naïve WT CD4$^{\square}$ T cells were activated under hypoxia for different times to assess cell death by
staining for 7-AAD/Annexin V. The line graph on the right showed percentages of apoptotic
cells. **B**. The time-course study as in **A** was repeated but with 50% of old media replaced by
fresh media every day. **C-D**. Naïve WT and HIF1α$^{-/-}$ CD4$^{\square}$ were activated under hypoxia for 3
days, with or without blocking antibodies against IL-2 (**C**), and with or without added IFN-γ (**D**),
followed by analyses of cell death by 7-AAD/Annexin V staining. **E**. Naive human CD4$^{\square}$ T cells
isolated from PBMCs of healthy donors were activated under hypoxia for 3 days, in the absence
and presence of 0.5mM 2-DG, followed by 7-AAD/Annexin V staining to detect cell death. All the
experiments were repeated at least twice. Pooled results shown in the dot plots depicted means
± SEM for all the samples in each group, with each dot denoting an independent sample. **,
p<0.01; ***, p<0.001; ****, p<0.0001. Source data were provided in the Source Data file.
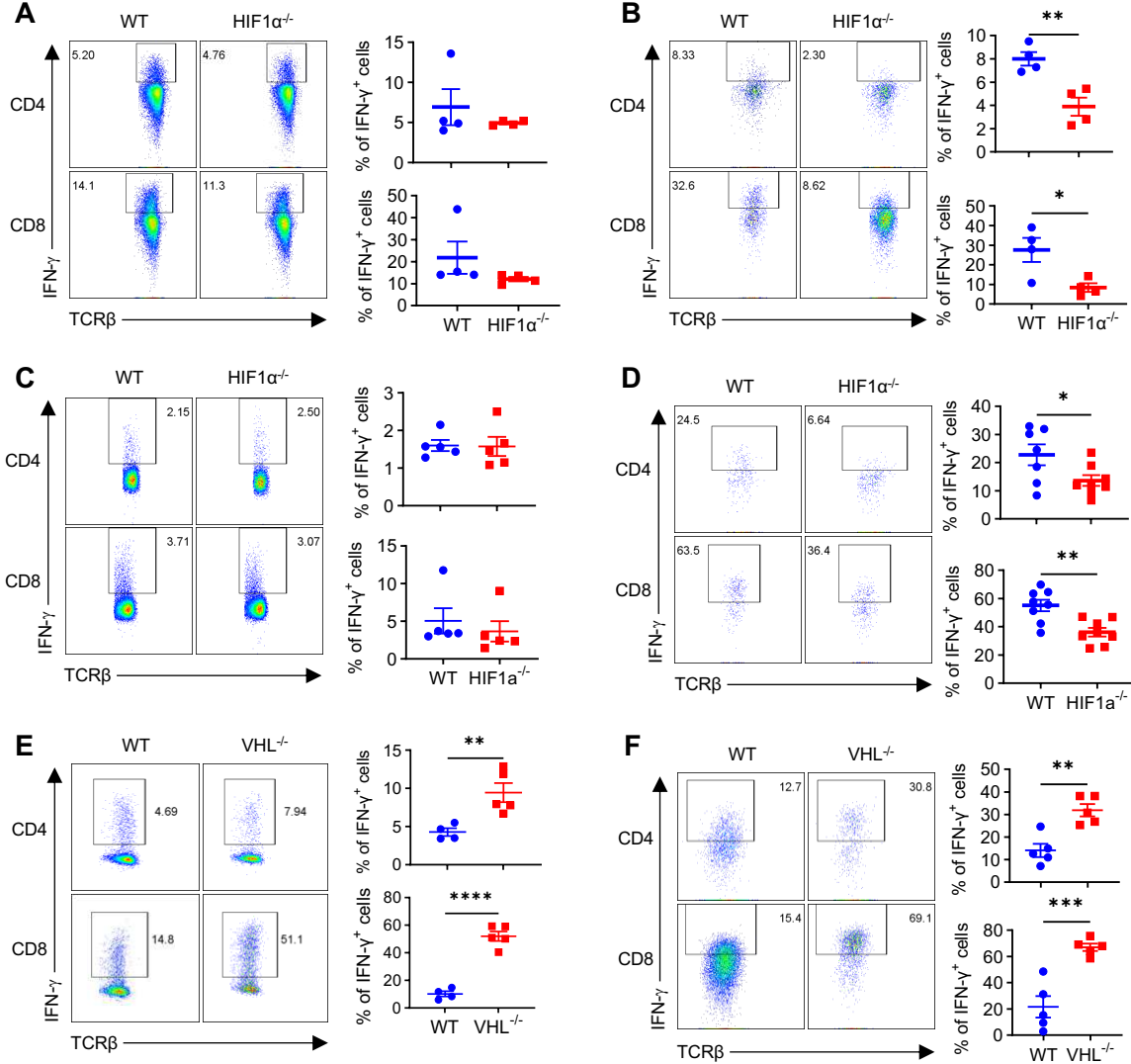
33

**Figure 5**



Figure 5. HIF1α regulates IFN-γ production in tumor-infiltrating T cells (TILs). A-B. T cells isolated from WT or HIF1α⁻/⁻ mice bearing established MB49 bladder tumor were analyzed for IFN-γ production by CD4$^\square$ and CD8$^\square$ splenocytes (**A**) or TILs (**B**). **C-D**. T cells isolated from WT or HIF1α⁻/⁻ mice bearing established orthotopic B16-BL6 melanoma were analyzed for IFN-γ production by CD4$^\square$ and CD8$^\square$ splenocytes (**C**) or TILs (**D**). **E-F**. T cells isolated from WT or VHL⁻/⁻ mice bearing established MB49 bladder tumor were analyzed for IFN-γ production by CD4$^\square$ and CD8$^\square$ splenocytes (**E**) or TILs (**F**). All the experiments were repeated 2-5 times. Pooled results shown in the dot plots depicted means ± SEM for all the mice in each group, with each dot denoting an independent sample. \*\*, p<0.01; \*\*\*, p<0.001; \*\*\*\*, p<0.0001. Source data were provided in the Source Data file.
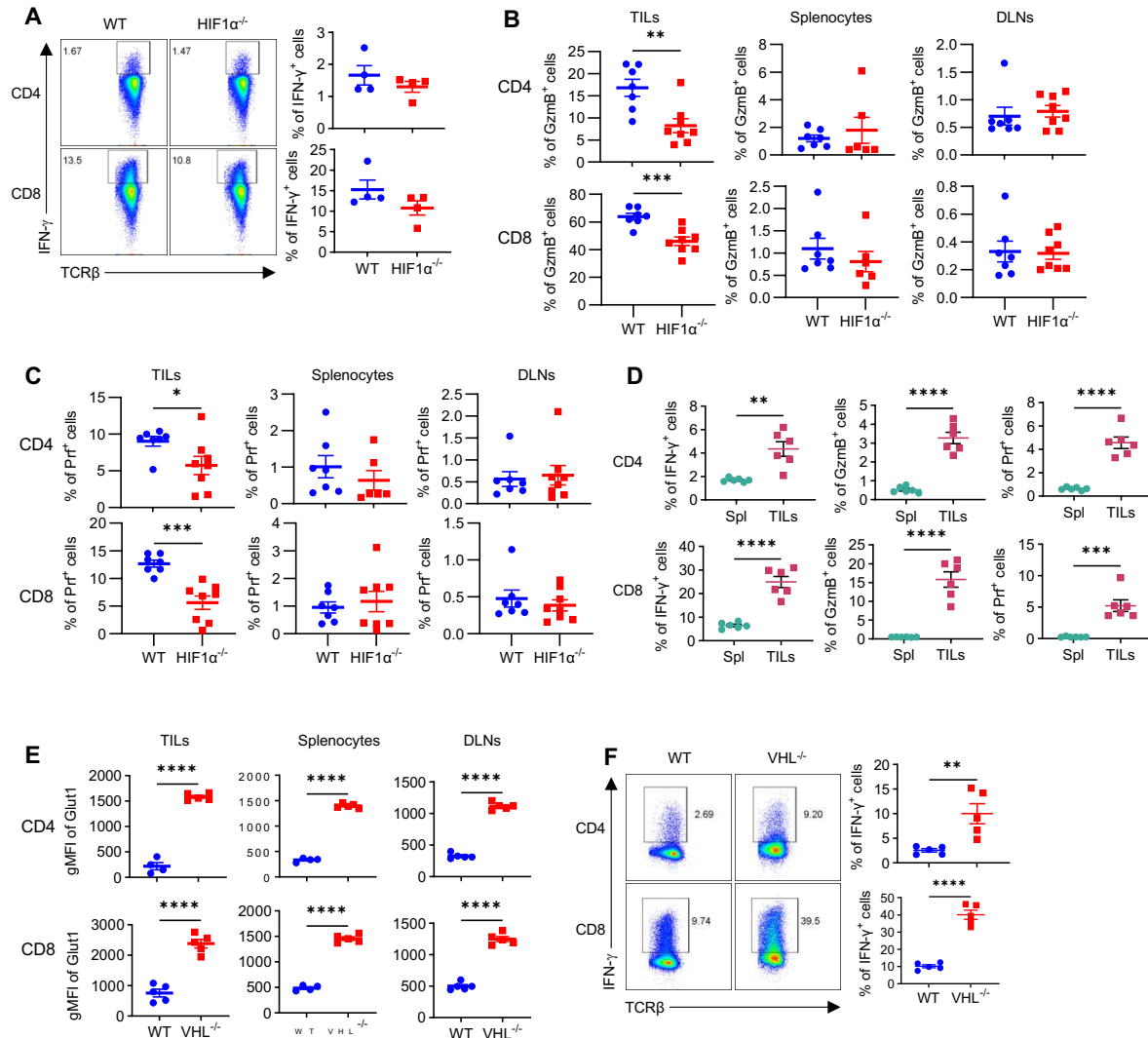
1155
1156  **Figure S5. HIF1α controls effector function of TILs. A**. T cells isolated from draining lymph
1157  nodes (DLNs) of WT or HIF1α⁻/⁻ mice bearing established MB49 bladder tumor were analyzed
1158  for IFN-γ production. **B-C**. Production of GzmB (**B**) and Prf (**C**) by CD4□ and CD8□ TILs or CD4□
1159  and CD8□ T cells from spleen and DLNs of WT or HIF1α⁻/⁻ mice bearing established MB49
1160  bladder tumor. **D**. Production of IFN-γ, GzmB, and Prf by CD4□ and CD8□ splenocytes vs CD4□
1161  and CD8□ TILs, isolated from WT mice bearing MB49 bladder tumor. **E-F** T cells isolated from
1162  WT or VHL⁻/⁻ mice bearing established MB49 bladder tumor were analyzed for Glut1 expression
1163  (**E**) in CD4□ and CD8□ TILs, splenocytes, and DLNs, as well as IFN-γ production by DLN CD4□
1164  and CD8□ T cells. All the experiments were repeated 2-5 times. Pooled results shown in the dot
1165  plots depicted means ± SEM for all the mice in each group, with each dot denoting a mouse. *,
1166  p<0.05; **, p<0.01; ***, p<0.001; ****, p<0.0001. Source data were provided in the Source Data
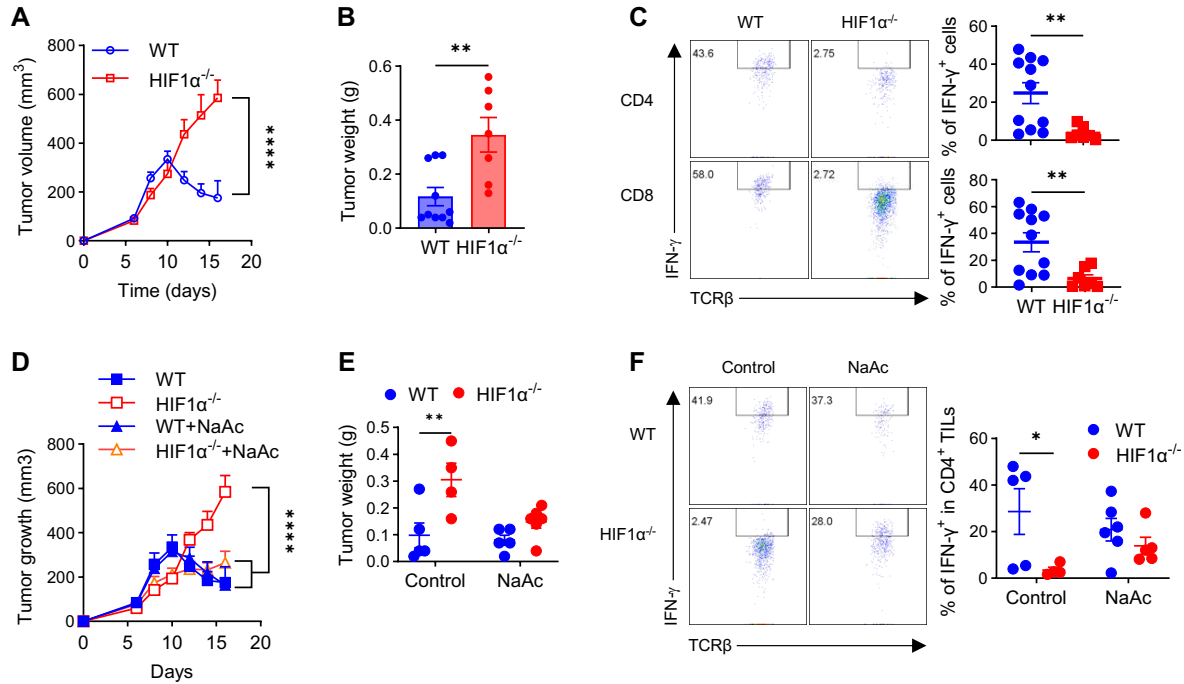1167  file.

**Figure 6**



1168
1169 **Figure 6. HIF1α in T cells governs therapeutic effects of ICBs. A-B**. WT and HIF1α$^{-/-}$ mice
1170 bearing palpable MB49 bladder tumor were treated with combined anti-CTLA-4+anti-PD-1
1171 therapy, followed by periodic measurement of tumor volume (**A**); upon euthanization, tumors
1172 were weighed (**B**).  **C**. IFN-γ production by CD4$^{\square}$ and CD8$^{\square}$ TILs isolated from tumor-bearing
1173 mice in **A-B**. **D-E**. WT and HIF1α$^{-/-}$ mice bearing palpable MB49 bladder tumor were treated
1174 with combined anti-CTLA-4+anti-PD-1 alone or in conjunction with administration of sodium
1175 acetate (NaAc), followed by periodic measurement of tumor volume (**D**); upon euthanization,
1176 tumors were weighed (**E**).  **F**. IFN-γ production by CD4$^{\square}$ TILs from tumor-bearing mice in **D-E**. All
1177 the experiments were repeated 2-5 times. Pooled results shown in the dot plots depicted means
1178 ± SEM for all the mice in each group, with each dot denoting a mouse. *, p<0.05; **, p<0.01;
1179 ****, p<0.0001. Source data were provided in the Source Data file.
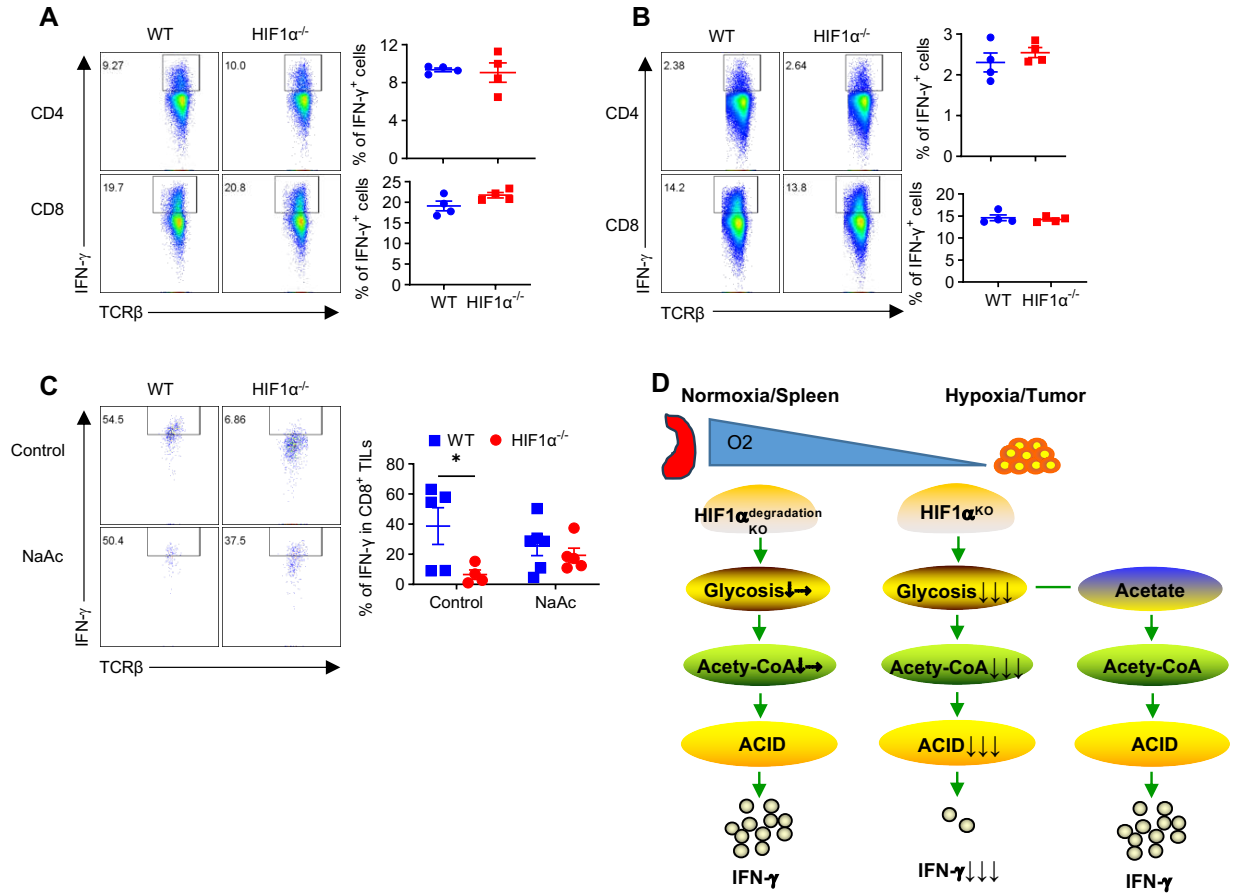
**Supplemental Figure 6**



1180
1181 **Figure S6. HIF1$\alpha$ in T cells governs therapeutic effects of ICBs. A-B**. WT and HIF1$\alpha^{-/-}$ mice
1182 bearing palpable MB49 bladder tumor were treated with combined anti-CTLA-4+anti-PD-1. IFN-
1183 $\gamma$ production by CD4$^\square$ and CD8$^\square$ T cells from spleens (**A**) and draining lymph nodes (DLNs) (**B**)
1184 was shown. **C**. IFN-$\gamma$ production by CD8$^\square$ TILs from MB49 bladder tumor-bearing WT and
1185 HIF1$\alpha^{-/-}$ mice treated with combined anti-CTLA-4+anti-PD-1 alone or in conjunction with
1186 administration of sodium acetate (NaAc). All the experiments were repeated 2-5 times. Pooled
1187 results shown in the dot plots depicted means ± SEM for all the mice in each group, with each
1188 dot denoting a mouse. *, p<0.05; **, p<0.01; ****, p<0.0001. Source data were provided in the
1189 Source Data file. **D**. A proposed model of how T cell-intrinsic HIF1$\alpha$-glycolysis controls IFN-$\gamma$
1190 production in hypoxic T cells.

37

**Supplementary Figure 7. FACS sequential gating/sorting strategies**

**FACS strategy 1:** for splenocytes, DLN, and cultured cells.
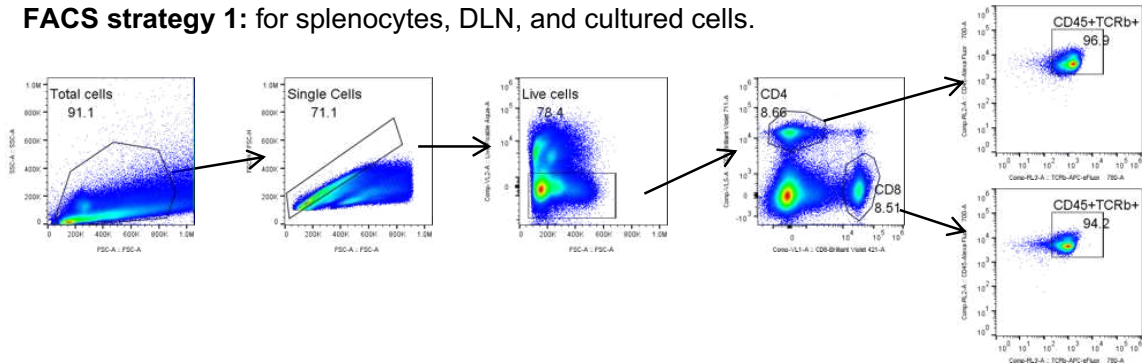


**FACS strategy 2.** for single cell suspensions of tumors.
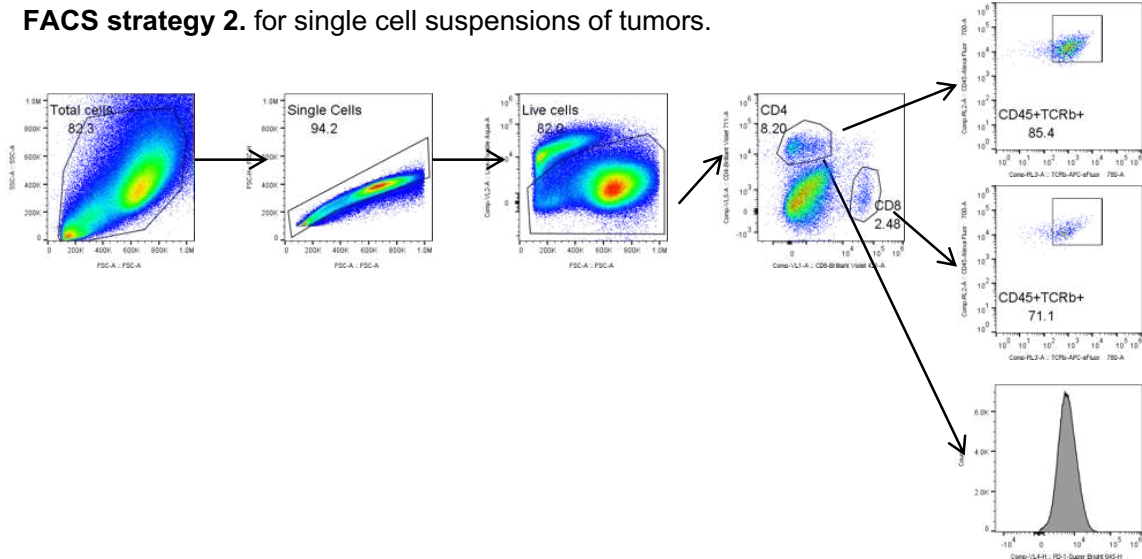


1191
1192

# Supplementary Files

This is a list of supplementary files associated with this preprint. Click to download.

- SupplTable1HypoxiaWTvsHIF1aKO.xlsx
- SupplTable2NormoxiaWTvsHIF1aKO.xlsx